TECHNICAL REPORT 1925
June 2005

Verification and Validation Report: Frequency Selective Surface Simulation Tool

T. Q. Ho
C. A. Hewett
SSC San Diego

D. A. Zolnick
M. Kragalott
D. J. Taylor
NRL

M. C. Baugher
NSWC, Dahlgren Division

A. K. Agrawal
Johns Hopkins University APL

SSC San Diego

TECHNICAL REPORT 1925
June 2005

Verification and Validation Report: Frequency Selective Surface Simulation Tool

T. Q. Ho
C. A. Hewett
SSC San Diego

D. A. Zolnick
M. Kragalott
D. J. Taylor
NRL

M. C. Baugher
NSWC, Dahlgren Division

A. K. Agrawal
Johns Hopkins University APL

SSC San Diego
San Diego, CA 92152-5001

SSC SAN DIEGO
San Diego, California 92152-5001

T. V. Flynn, CAPT, USN
Commanding Officer

R. F. Smith
Executive Director

ADMINISTRATIVE INFORMATION

This report was prepared for the Naval Sea Systems Command PMS 500 DD(X) Program Office by the Photonics and RF Technology Branch (Code 2825), Space and Naval Warfare Systems Center San Diego; the Naval Research Laboratory; the Naval Surface Warfare Center, Dahlgren Division; and the John Hopkins University Applied Physics Laboratory.

Released by
W. Henry, Head
Photonics and RF
Technology Branch

Under authority of
D. M. Gookin, Head
Network & Information
Systems Division

ACKNOWLEDGMENTS

The authors of this report gratefully acknowledge the following persons for their important contributions to the VIPER I project in general and specifically for their efforts towards completion of the research and validation effort described in this report.

We would like to thank Michelle Bui of the Space and Naval Warfare Systems Center San Diego (SSC San Diego) and Shawn Allen of the Naval Surface Warfare Center, Dahlgren Division, who contributed to the code debugging and validation effort. We also extend our thanks to a group that provided excellent technical guidance for the entire project, including Mr. Steven Hart, formerly of SSC San Diego; Dr. William Pala of the Naval Research Laboratory; Dr. Thomas Cwik of the Jet Propulsion Laboratory; and Mr. Ray Allen of Symmetron, Inc., who also provided valuable editorial assistance with the final report.

The project could not have been accomplished without the support of Capt. Charles Goddard, Program Manager DD(X), PMS 500; the former head of PMS 500, RADM Tom Bush; and the Technical Directors associated with PMS 500, including Capt. Charles Behrle, Capt. Jim Wilkins, and Capt. Kenneth Webb, USN (ret). Finally, we recognize and acknowledge the dedicated efforts of our sponsor, Mr. Thomas Ready, the Program Manager for Integrated Topside Design research and development, who funded this project; the PMS 500 financial support staff; and Mr. Herbert Williams and Ms. Naomi Silver, who made sure the necessary resources were available when needed.

EXECUTIVE SUMMARY

To address the shortfall in modeling and simulation (M&S) software capabilities for modeling radomes of various types, PEO-DD(X)/PMS-500 commissioned the development of a plan to satisfy these needs. Frequency Selective Surface (FSS) M&S was identified as one of the most promising FSS simulation approaches, and was selected for further development. This report presents a summary of the verification and validation (V&V) of the enhanced FSS M&S code over a wide range of electromagnetic (EM) test cases, including infinite and finite structures.

Numerous infinite FSS element classes were evaluated with FSS during this V&V, including dipole elements, loop-type elements (circular, square, hexagonal, and cross), gridded loops, and slot elements (cross and tripole). FSS structures consisting of elements printed on single, thin dielectric substrates were considered, as were structures with multiple dielectric layers encapsulating the FSS. FSS structures with multiple FSS layers were also analyzed. These structures included cases where the FSS unit cells were identical or incommensurate. The FSS M&S results compare favorably with measured data and alternative numerical techniques.

Selected FSS structures were further analyzed using the finite FSS M&S tool. Again, gridded structures, loop elements, and slot elements were considered. The radome characteristics predicted by the finite FSS M&S tool showed excellent agreement with the measured data. Based on the cases examined here, one finding is that finite FSS arrays as small as 7 x 7 in extent can be adequately approximated by the infinite solution.

The FSS M&S V&V conducted under this study was extensive, and was a significant success. Of the 16 cases investigated, 9 cases have numerical and measured results for comparison. Each test case considered was selected to verify FSS M&S performance for a specific application or to validate the underlying theoretical framework of the M&S package. No example studied produced less than favorable results. Throughout this study, FSS M&S demonstrated that it could accurately predict the performance of a wide range of radome structures. Based on the reported results, FSS M&S has been verified and validated as a capable FSS radome M&S tool for use in the DD(X) program.

CONTENTS

Figures

Tables

1. BACKGROUND

1.1 USER NEED

The DD(X) design teams were tasked to develop radio frequency (RF) apertures that satisfy low observability and high-bandwidth requirements. The technology that meets the design requirements may include phased array antennas located near frequency selective surface (FSS) radomes. The teams' primary concerns are the design, analysis, and synthesis of novel FSS structures. They must accurately predict radome transmission and electromagnetic (EM) energy reflection to achieve DD(X) design goals.

Users will require a computational tool that provides the following:

- Computer-assisted design (CAD) of FSS elements composed of various materials
- An arbitrary specification of incident electromagnetic energy wavefronts
- Synthesis algorithms to rapidly develop novel bandpass structures

Successful modeling and simulation (M&S) software must include the following features:

- Accurate prediction of electromagnetic scattering in the presence of finite FSS radomes that contain arbitrarily shaped structures made of complex materials
- Library of radome designs and a method to specify arbitrary structures in a CAD environment
- Available data outputs with the current FSS distribution, reflection, and transmission coefficients
- Efficient and intuitive user interface that promotes rapid design development

1.2 M&S DESCRIPTION

The FSS Simulator (hereafter referred to as FSS M&S) combines EM analysis and layout to provide a powerful solution for analyzing general FSS. FSS M&S includes an extensive collection of standard elements and models arbitrary FSS elements. The enhanced FSS M&S is based on a commercial off-the-shelf product developed by RM Associates (RMA). RMA also developed ability to model finite FSS structures.

1.3 M&S SOFTWARE METHODOLOGY

FSS M&S will provide a solution to the user need described in Section 1.1. A fully functional FSS M&S system installation requires a desktop computer running the Microsoft Windows® operating system, the FSS software package that RMA is developing for the Navy, and the examples and operational notes developed during this verification and validation (V&V) study. The complete software package will be available for purchase from RMA upon completion of the current contractual upgrades. The FSS M&S software developer and the V&V agent will also provide technical support. The FSS M&S software developer will also provide a user instruction manual that includes tutorials and example simulations on current radome research. M&S users will have access to the test cases that were used to verify and validate the FSS M&S software, including documentation and source files. These test cases will include standard problems from FSS radome theory. The FSS M&S software users will accomplish system installation on-site.

2. PERFORMANCE

2.1 REQUIREMENTS TESTING MATRIX

The performance of V&V activities is based on satisfying acceptability criteria. Linking the V&V tasks to acceptability criteria, which are in turn traced to the M&S user requirements, ensures that the scheduled V&V tasks are sufficient to fully validate the M&S system. This process ensures that the verification, validation, and accreditation (VV&A) program budget and schedule are met. Table 1 shows the FSS M&S requirements testing matrix.

Table 1. Requirements testing matrix.

#	Acceptability Criterion (V&V agent documented evidence)	Measures & Metrics	V&V Task Planned to Satisfy Acceptability Criteria
1	Accurately predict the performance of general infinite FSS structures	Transmission and reflection coefficients	Representative test cases will be constructed and validated against measurements and alternate simulations
2	Accurately predict the performance of general finite FSS structures	Transmission and reflection coefficients	Representative test cases will be constructed and validated against measurements and alternate simulations
3	Provide an efficient and intuitive user interface	Time required to set up, simulate, and analyze results	The entire setup, simulation and analysis procedure will be documented and analyzed for efficiency

2.2 CONCEPTUAL MODEL VALIDATION

The FSS M&S software simulates EM radiation scattering from a two-dimensional periodic array of conducting elements. Users can choose the size, shape, and orientation of the conducting elements to produce frequency-dependent scattering of the incident energy. This characteristic makes FSS highly useful in a multifunctional communications system.

The theoretical analysis of a single-screen FSS begins with the understanding that a large periodic array can, to a first approximation, be considered infinite. In this situation, the Floquet theorem [1] allows the solution of the entire system to be determined from the solution of a unit cell with periodic boundaries. This concept greatly reduces the required computational resources. At the conducting surface in the unit cell, the incident fields are related to the surface current density using the fact that the tangential electric field at the conductor vanishes. Therefore, the reflected tangential electric field must exactly cancel the incident tangential electric field at this surface. The reflected field is related to the current density by the Green's function [2] for EM energy propagating in free space (no dielectric is present yet). The current density can be expanded in a suitable set of basis functions. The system is then converted to a matrix equation for the coefficients of the basis function expansion by forming the scalar product with a test function. The resulting linear system of equations can be solved by using standard techniques to obtain the coefficients and, thus, the current that the incident field induced in the conductor.

The solution technique discussed above can be extended to compute incident radiation scattering by multiple FSS screens embedded in dielectric media. In this configuration, the incident fields will induce currents in several different conductors and the total scattered

fields must include a contribution from the conductors in each layer. Dielectric and conducting material close to the radiating currents requires constructing a new Green's function that reflects the complex boundary conditions. The Green's function can be obtained by using the spectral-domain immittance approach. In this analysis, the problem is transformed to the Fourier domain, where a suitable change of coordinates decouples the integral electric field equations into transverse electric (TE) and transverse magnetic (TM) cases. This decoupling allows the system to be formulated in the context of transmission line theory. The spectral Green's functions for multilayered dielectric structures are then obtained by repeated applications of the transmission line equations.

The analysis techniques described above encompass the computational engines used in legacy FSS M&S software. In particular, the simulation software packages currently available are limited to infinite arrays of elements illuminated by plane waves. However, the FSS radomes used in communications systems are often operating in the near-field region of antennas, and finite size effects may be important. In the FSS M&S, a novel approach is used to model truncated FSSs illuminated by a plane wave. The original truncated problem is transformed into an equivalent one that preserves its periodicity and renders it far more manageable and numerically efficient to treat than the original version. In the equivalent problem, FSS is still infinite and doubly periodic, but the illumination function is windowed such that it illuminates only the truncated portion of the radome. This situation requires an infinite FSS solution for each spectral component of the plane wave representation of the windowed illumination. However, this problem is far more practical to analyze than the original one involving the truncated FSS, especially for large radomes.

To verify the functional completeness of this conceptual model, the V&V agent will characterize the effects of FSS radome truncation and near-field excitation on various systems. The results will be compared to available data to determine the accuracy of the finite array-plane wave analysis extensions included in the FSS M&S. The assumptions and algorithms used in the theoretical developments of the FSS M&S software computational engine will also be examined for technical justification. The final result of this study will be an assessment of the functional adequacy of the M&S software. The significance of the corrections that the FSS M&S provides on the overall system performance will determine the acceptability criteria for the accuracy of the theoretical models.

2.3 FUNCTIONAL VERIFICATION

The functional implementation of the FSS M&S conceptual model consists of an integrated design environment that allows the user to quickly and easily design unit cell dimensions, array size, and incident wavefront scattering analysis in a Microsoft Windows®-based interface. The FSS M&S software also provides a genetic algorithm for synthesis of new radome structures based on performance metrics. The user selects source excitations and output field designations. The FSS M&S then performs the necessary computations and outputs data.

The verification of the functional design consisted of evaluating the ease with which problems are defined when using the FSS M&S. Finite array truncation effects were quantified. Array size was varied and compared to the infinite solution to determine under what conditions the finite FSS could be approximated as an infinite FSS. Each specific category of FSS radome simulation defined in the conceptual model was verified in separate test cases. The simulations represented a cross-section of the structures handled by the FSS M&S computational engine. These individual test cases provided a check on the validity of each element in the functional implementation. Additional test cases, which include all relevant

categories of radome applications, were analyzed to determine the effectiveness with which the FSS M&S functions are used across a broad range of problems. Finally, the range of output data options was investigated to determine whether the needs of the FSS M&S software user were satisfied.

A design walk-through was performed at the conclusion of the new software development and the V&V agent received instruction on using the M&S software package. The M&S software developer demonstrated the new system and presented an outline of the structure and function of each new tool.

2.4 SYSTEM VERIFICATION

Space and Naval Warfare Systems Center San Diego (SSC San Diego) personnel performed the system verification and base-level checks on the algorithms used in the FSS M&S software. These test results confirmed the proper functional implementation of the conceptual models. During test case valuation, the FSS M&S software was compared with contemporary engineering and Department of Defense (DoD) standards of structure and documentation. System reliability was also quantified during test case construction and simulation.

FSS M&S software system effectiveness was determined during the results validation. SSC San Diego evaluated and reviewed the default installation procedure and training manual. The V&V agent identified program bugs, instruction manual misprints, and repetitive or illogical procedures. The agent was also responsible for documenting any M&S system failures and/or peculiarities during the results validation.

2.5 RESULTS VALIDATION

Designers used the FSS M&S program to construct test models and compute RF energy scattering. The results were compared to measured data and alternate simulations in the open literature. Some test cases were chosen to verify FSS M&S software performance in a specific area of user need. In other cases, the underlying theoretical framework of the FSS M&S software was validated. The results of the test case simulations were compared to analytic results, experimental measurements with existing FSS radomes, and numerical data from other numerical routines. The results were expected to agree within a standard 10 percent margin of error.

3. TEST CASES

Frequency selective surfaces are simply a two-dimensional periodic array of patch or aperture-type elements. The terminology reflects the intrinsic frequency-dependent filtering characteristics that such structures exhibit. Adding dielectric layers and cascading multiple FSSs into a composite structure modifies FSS properties. A major FSS application is radome design. Conventional radomes are intended primarily for weather protection and use RF transparent dielectrics. However, adding an FSS to the radome structure provides a significant additional degree of control. The radome can be designed to allow an RF signal to propagate through while rejecting any undesired out-of-band signals. The design also allows control of backscattered fields and thereby lowers radar profile. An appropriate design can be used to tailor the frequency response of the composite radome to provide band-stop or band-pass filtering characteristics. Besides the radome application just mentioned, antenna systems [3] based on FSS dichroic subreflectors can be used to realize multichannel operations. The subreflector allows signal multiplexing from multiple reflector foci, which leads to a significant weight reduction, particularly in spacecraft applications.

The V&V test cases discussed in this section represent a broad cross-section of FSS structures that are useful for engineering applications. Infinite structures were considered first because they are simple mathematically. These structures included various elements such as gangbuster type surfaces, concentric rings, square loops, tripoles and cross-slot types, and dielectrically loaded crosses and hexagonal ring biplanar structures. Next, finite structures, including gridded square-loop elements, tri-slots, and cross-slots, were analyzed. The FSS M&S was used to simulate all cases, and corresponding results were compared to measurements, analytical formulas, and alternative software packages.

Assumptions. The FSS M&S is based on the scattering matrix technique. The computational engine uses a spectral-domain approach for analyzing the plane-wave response of the planar, periodic FSS structure. An accurate solution requires a suitably fine spatial resolution. In general, we will assume that small (<5%) differences in the results upon doubling the spatial resolution will constitute a convergent solution. The conducting elements in the FSS structures are also considered infinitesimally thin. This assumption is valid when the RF energy absorption is localized within the conductor skin depth. For the test cases examined in this report, the material properties of the supporting structures in the simulation are considered isotropic and independent of frequency over the simulation operating range.

Procedures. In general, the technique used to validate this M&S will be to compare results from FSS structures modeled with the FSS M&S and alternative M&S tools, as well as measured data (where available). The FSS is characterized by its reflection and transmission coefficients as functions of frequency and incidence angle. The reflection coefficient represents the incident power reflected away from an FSS back towards the input source. The transmission coefficient represents the power that is transmitted through the FSS to the other side. A radome protecting an antenna should have a high transmission coefficient within the antenna's band of operation while exhibiting a high reflection coefficient elsewhere to achieve out-of-band rejection. Current distribution patterns on the FSS surface are also available.

Application Note. The FSS M&S version 1.2 distribution package consists of a single .zip file. Unzipping the distribution file produces the following seven files:

File name	File size (bytes)
0x0409.ini	4,632
Data1.cab	9,328,394
FSS v1.2 – Spawar (A-c).msi	975,872
instmsia.exe	1,708,856
instmsiw.exe	1,822,520
setup.exe	225,638
Setup.ini	1,223

Installation proceeds by executing the setup.exe file. The default installation location is a subdirectory named “FSS” in the “Program Files” directory. It is recommended that the user accept the default location and name. The completed installation will have 18 files in the “FSS” subdirectory:

File name	File size (bytes)
DeIsL1.isu	3,538
dissimilarfss.exe	651,264
Finite_FAR_MOD.exe	270,336
Finite_FSS_MOD_CUR.exe	266,240
FINITE_FSS_PLANE_WAVE.bat	90
FINITE_FSS_Plane_Wave.exe	557,056
fss.exe	2,662,400
FSSDisplay.exe	974,848
FSS_Help.chm	3,095,286
GAFSS01.exe	507,904
GAFSS2.exe	638,976
INF_FSS_PLANE_WAVE.exe	458,752
Process_Cur.exe	266,240
Process_Far2D.exe	266,240
Process_Far3D.exe	286,720
projectname.txt	214
_DEISREG.ISR	147
_ISREG32.DLL	47,104

The simulation process begins by selecting a project type and is followed by parameter specification. As part of the layout, a three-dimensional unit cell is defined and forms the basis for modeling the entire FSS radome structure. After the project input files are created, the simulations are executed. Upon completion, the built-in visualization features can be used to evaluate the performance of the constructed FSS structure.

Input for each FSS solver is processed through a Graphical User Interface (GUI). The GUI includes a help file. Within the GUI, the user first chooses the type of project from a drop-down menu. The units (i.e., MHz, GHz, mils, inches, etc.) are then specified. Subsequent selections include unit cell size, unit cell discretization, and selection of incidence angles and frequency. The GUI then presents a design window in which the user builds the FSS structure layer by layer. The incident energy is assumed to impinge on layer 1 of the FSS cross-

section. Materials properties are also input during this process. A library of typical FSS elements is available, or more complicated elements can be built using library elements. A drawing option can be used to form elements of arbitrary shape. Various view angles are available to aid in the design process. Existing project files may also be opened and examined or revised.

When the FSS design is completed, the project is written to disk. Project files are stored as ASCII text files. The experienced user can quickly modify inputs by editing the appropriate text files. After saving the project files, the GUI presents a review window that shows the FSS structure cross-section. Selecting the FSS layer displays a plan view of the FSS unit cell. Within this view, regions covered by metallization appear in red while regions with no metallization are white. This view helps determine whether a sufficient level of discretization has been implemented and the amount of staircasing that is present. It is important to note that although the unit cell is depicted as a square in this view, the x and y steps may be different dimensions. Thus, a circle may appear as an ellipse in this view.

Upon exiting the review window, the user may select the GUI "Simulation" tab. A drop-down menu presents the available simulation types. Selecting the appropriate type initiates the simulation within a DOS-type window. Once the simulation is finished, the results are written to a text file. Intermediate results are written as they are calculated. The GUI provides basic visualization tools to allow rapid evaluation of the results. The user may also use more advanced graphing and evaluation tools such as Microsoft Excel or MATLAB® for further evaluation.

3.1 INFINITE FSS CASES

By definition, a periodic structure is infinite in extent. In reality, all fabricated FSS structures are finite in size. However, it is mathematically easier to model an infinite structure than a finite structure. It is generally assumed that the resulting infinite model provides a reasonably accurate picture of the finite FSS properties, particularly for FSS arrays containing large numbers of the unit cell. In this section, as the first part of the verification and validation of the FSS M&S tool, we examine the performance of 12 infinite FSS examples.

3.1.1 Gangbuster Type 2 Surface

The gangbuster surface belongs to the FSS class consisting of center-connected elements. It consists of straight dipole segments arrayed on a grid with periodicity, D_x and D_y. Figure 1 shows a grid where $D_x = D_y$. (The dots simply represent grid points, not components of the FSS.) A "type n" surface is defined as one in which one end of the dipole is located at (x, y) and the other is located at ($x + D_x$, $y + nD_y$) [4]. The dipole elements are typically arranged to minimize the onset of grating lobes (dependent upon D_x, D_y, and the incident angle). A single gangbuster surface (Figure 1) can handle only linear polarization. The unit cell, which can be stepped in the x and y directions to reproduce the entire surface, is outlined in red. Adding a second identical gangbuster surface rotated 90° to the first surface allows arbitrary polarization. This particular FSS screen has the passband within the Ku-band for TM mode.

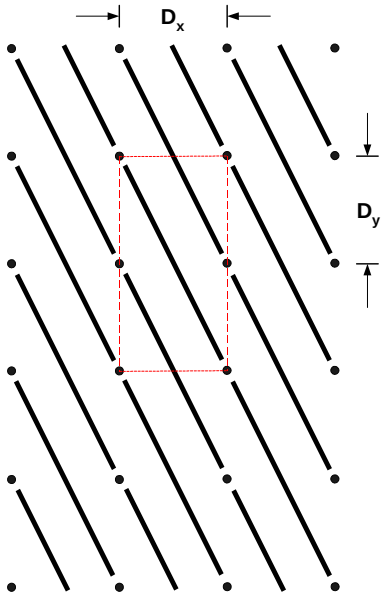

Figure 1. Gangbuster type 2 surface.

Figure 2 shows an enlarged view of the unit cell used for this simulation with the dimensions specified [4]. The unit cell consists of one simple straight dipole and two partial dipoles. The cell is replicated periodically in two orthogonal directions in a planar configuration. The FSS dipole elements are sandwiched between two identical 20-mil dielectric sheets. The dielectric constant of these sheets is 2.2, typical for a duroid substrate. Within the FSS code, the FSS elements are treated as infinitely thin, perfect electrical conductors (PEC material). Copper is a typical choice for conductor metallization. In practice, a typical printed element thickness will be on the order of 0.5 to 1.5 mil, depending on the power-rating requirements. Thicker elements are required to support higher power levels.

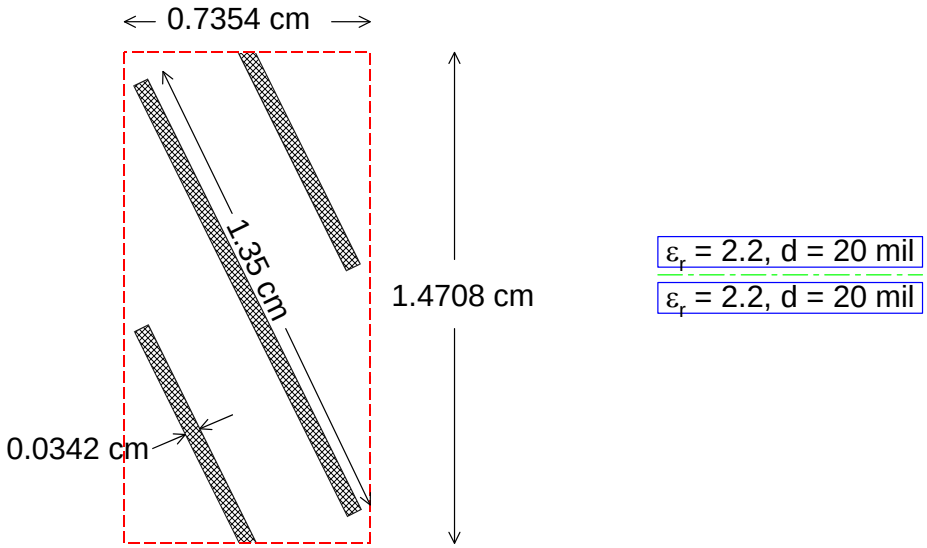

Figure 2. Unit cell and cross-section used within FSS simulation.

Figure 3 shows the FSS screen as approximated by four different unit cell discretizations from 32 x 32 to 256 x 256. Increasing the unit cell discretization provides a more precise representation of the gangbuster element and therefore more accurate performance data at the expense of an increase in computation time. Figure 4 data had a unit discretization of 128 x 128. The discretization selection is a compromise between reducing staircasing along the dipole sides and minimizing the simulation runtime.

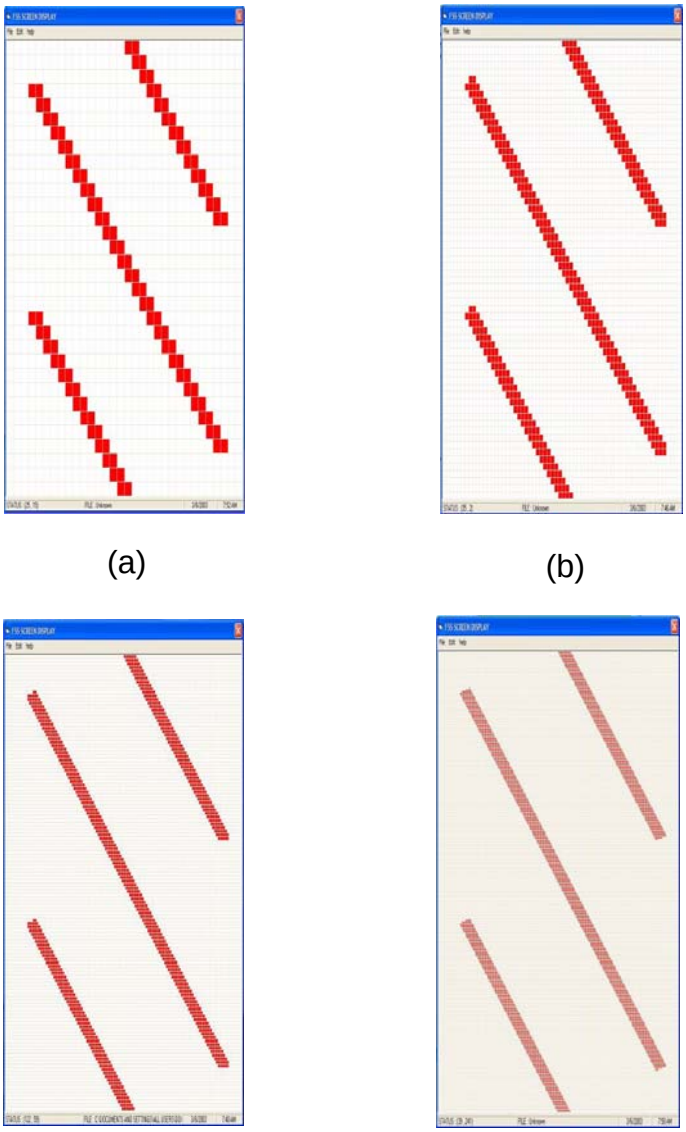

Figure 3. Unit cells (a) 32 x 32, (b) 64 x 64, (c) 128 x 128, and (d) 256 x 256 discretization.

The first FSS propagation characteristic considered is the reflection coefficient. The reflection coefficient is simply the ratio of the reflected power to the incident power. Reflection coefficients as a function of frequency were calculated for an incidence angle θ of 45°, but with rotation angles ϕ of 26.6 and 116.6° for TE and TM polarizations using FSS code (infinite engine). Polarization is a property of a single-frequency EM wave; it describes the shape and orientation of the field vectors as a function of time. TE and TM polarizations are rotated 90° in physical space. The case results are compared with those obtained by using Periodic Moment Method (PMM) [5], an alternative simulation tool. Figure 4 summarizes the results obtained with both codes. TE and TM polarizations are shown at two different rotation angles (ϕ = 26.6° and 116.6°) for incidence angle, θ = 45°. The FSS and PMM calculations are essentially indistinguishable at low frequency for each of the four (rotational angle and polarization) cases, with excellent agreement at higher frequencies. Resonant frequencies determined for the ϕ = 116.6° with TM polarization case differ by only 2%, which in this example, corresponds to the frequency step size (0.27 GHz) used in the simulations. The maximum deviation is at ϕ = 26.6° with TM polarization. Here, the two curves are still separated by less than 1 dB. However, the reflection coefficient is –20 dB or less over the designated frequency band, so this difference is negligible.

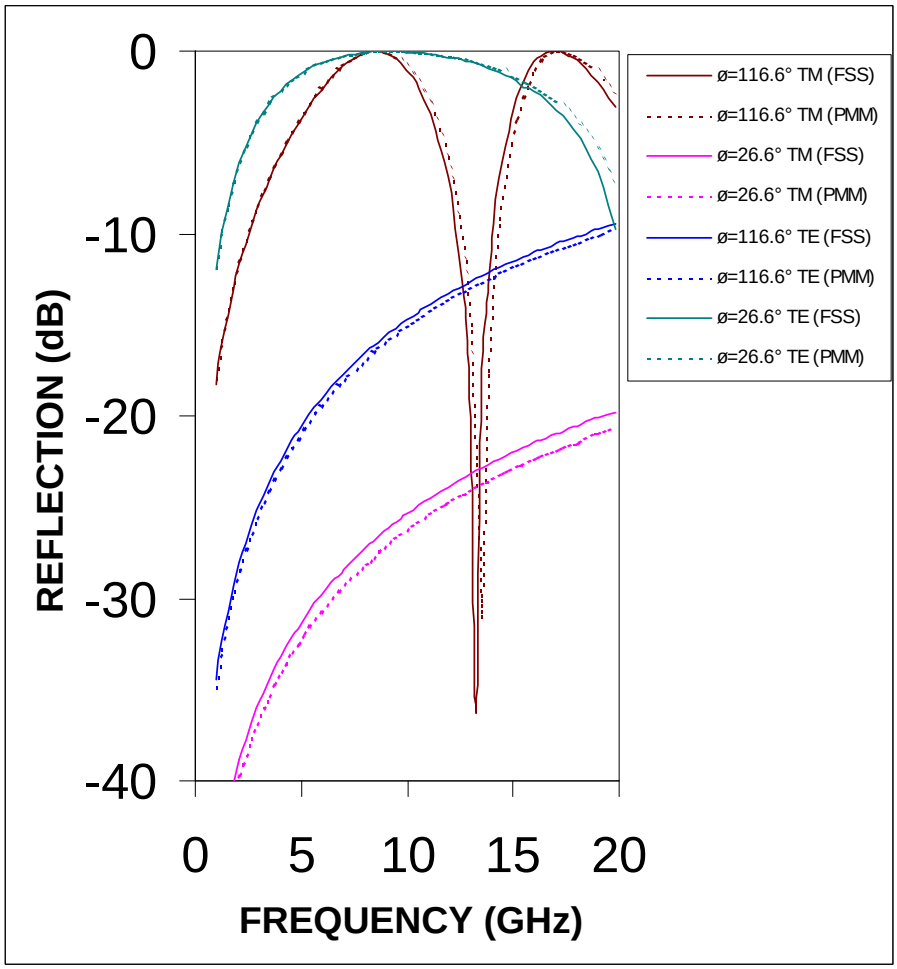

Figure 4. Reflection coefficient as a function of frequency (θ = 45°).

3.1.2 Gangbuster Type 4 Surface

The gangbuster type 4 FSS consists of simple, straight dipoles arrayed on a square grid (Figure 5). The difference between this case and the previously described gangbuster type 2 is that now n = 4. This concept is implemented to produce a linearly polarized field. This particular FSS screen [6] is designed to have a TM mode passband within the Ku-band. This design is accomplished by keeping the dipole length at 1.35 cm, as in the previous test case, while reducing the D_x and D_y spacings.

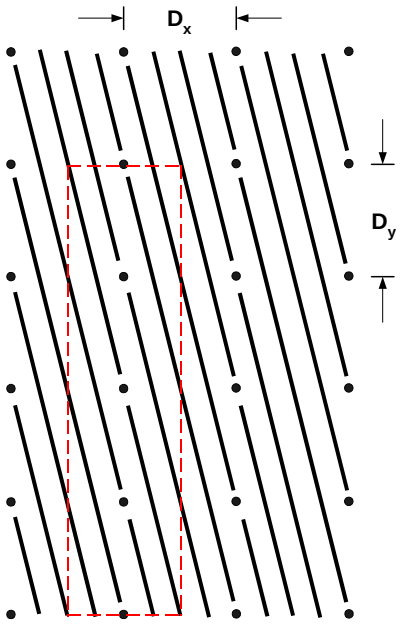

Figure 5. Gangbuster type 4 surface.

Figure 6 shows a detailed view of the unit cell used for this simulation with the dimensions specified [6]. The cell consists of 11 partial straight dipoles and is replicated periodically in two orthogonal directions in a planar configuration. The FSS dipole elements are sandwiched between two identical 20-mil dielectric sheets. The dielectric constant of these sheets is held at 2.2. Within the FSS code, the FSS elements again consist of infinitely thin perfect electrical conductors (PEC material). Figure 7 shows the FSS screen as approximated by a 128 x 128 unit cell discretization.

As in the previous case, FSS code was used to calculate reflection coefficients as a function of frequency for a single incidence angle ($\theta = 45°$) and two rotation angles ($\phi = 14°$ and 104°) for TE and TM polarizations as a function of frequency. For validation, the data from the FSS calculation were compared to an alternative simulation (PMM) based on the method of moments. Figure 8 shows the reflection coefficient as a function of frequency over the 0- to 20-GHz frequency span for TE and TM polarizations at an incidence angle $\theta = 45°$ and with rotation angles $\phi = 14°$ and 104°. The FSS and PMM calculations are essentially indistinguishable over the entire frequency range for $\phi = 14°$ TE, with both calculations showing the FSS as an excellent reflector between 3 and 18 GHz. Similar agreement is seen for $\phi = 104°$ TM, which again shows the FSS as an excellent reflector, but with the FSS code predicting a narrow transmission window or null at 12.4 GHz. PMM predicts the minimum at

12.5 GHz, a difference of less than 1% and within the step-size resolution for the two simulations. For the $\phi = 14°$ TM and $\phi = 104°$ TE cases, the two codes predict similar trends. Each case predicts low (<–30 dB) reflection coefficients at low frequency, gradually increasing to –20 dB and –10 dB, respectively at 20 GHz. A modest offset of ~ 1.6 dB exists between the two $\phi = 104°$ TE simulations, and an ~3-dB offset exists between the two $\phi = 14°$ TM predictions. The reflection coefficient magnitude is –15 dB or greater at the center frequency.

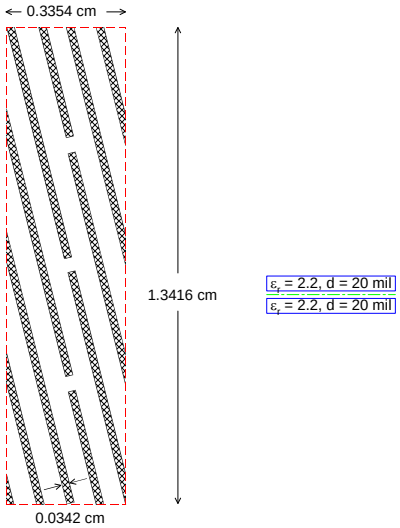

Figure 6. Unit cell and cross-section used within FSS simulation.

Figure 7. Gangbuster type 4 unit cell with 128 x 128 discretization.

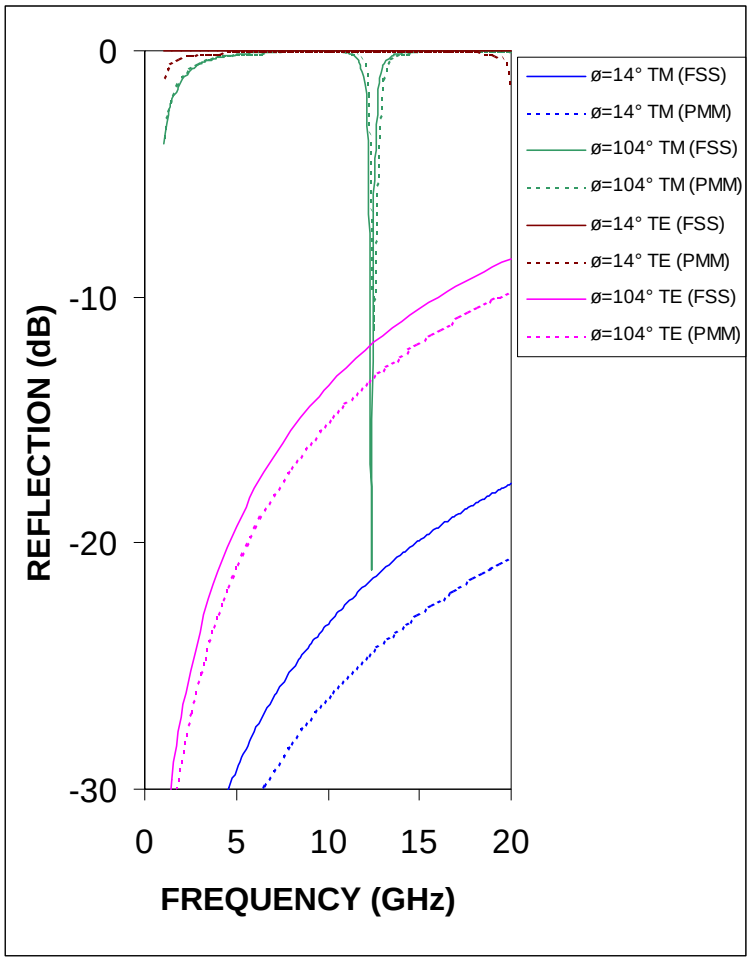

Figure 8. Reflection response for gangbuster type 4 surface (θ = 45°).

3.1.3 Single-Screen Ka-Band FSS with Double-Ring Patch Elements

In the next test case set, we consider a different class of elements, the loop type. In these cases, we examined the performance of an FSS that has a unit cell consisting of multiple elements, particularly concentric circular rings. The first case was the Ka add-on FSS; this test case analyzed a single FSS screen in which two circular loops form the basic element. The FSS in this example passed S-/X-/Ku-band signals while providing a high degree of rejection in the Ka-band. Figure 9 shows the elements arranged on a grid with a 60° skew angle. A single freestanding ring will resonate when the wavelength is equal to the ring circumference, providing a rejection band. Dielectric loading causes the resonant frequency to decrease as the dielectric constant of the substrate is raised. Adding a second closely sized ring adds a second resonance frequency. Combining the two provides a higher Q performance to achieve high rejection within the stop-band. Annular elements have rotation symmetry, and thus provide uniform transmission response for circularly polarized incident beams. Figure 9 highlights the unit cell (on a non-skewed grid) in red. The figure also shows that the double-ring patch element array is patterned on a 2-mil kapton sheet. Dimensions are D = 0.169 inch, r_1 = 0.047 inch, r_2 = 0.028 inch, and $W_1 = W_2$ = 0.010 inch [7]. Note that r_1 and r_2 are the average of the inside and outside radii of each ring. Figure 10 shows the unit cell as modeled within FSS.

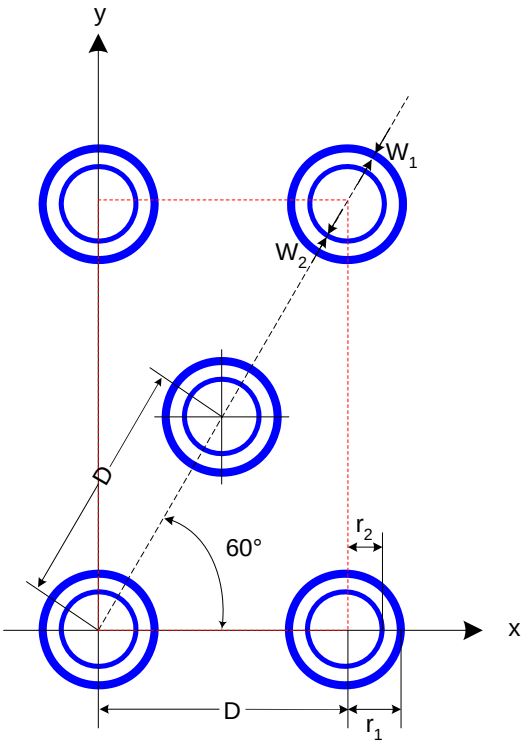

Figure 9. Unit cell consisting of dual rings arranged on triangular grid.

The FSS M&S code infinite analysis option for TE and TM polarizations at several incidence angles (27- to 35-GHz frequency range) was used to calculate the reflection transmission coefficients. The results for this case are compared with measured data and results in the open literature.

Figure 11 shows representative data for an incidence angle of 30° when using TE polarization and shows the transmission coefficient as a function of frequency from 27 to 35 GHz. A solid blue line shows data calculated by using FSS. A dashed blue line plots the predictions from the modal analysis described in reference [8]. The red plot shows measured data. The FSS-predicted response of the Ka add-on FSS shows a null centered at 32.6 GHz, while the measured data indicate 33 GHz, a difference of ~1.2%. The rejection characteristics are also similar. The results from both simulations show good agreement for this particular FSS design. Figure 12 presents transmission data for TE (blue curves) and TM (red curves) polarizations with a 45° angle of incidence. The solid lines are the FSS M&S predictions, while the dashed lines are the corresponding modal analysis data. Again, agreement between the two simulation techniques is excellent over the entire frequency range.

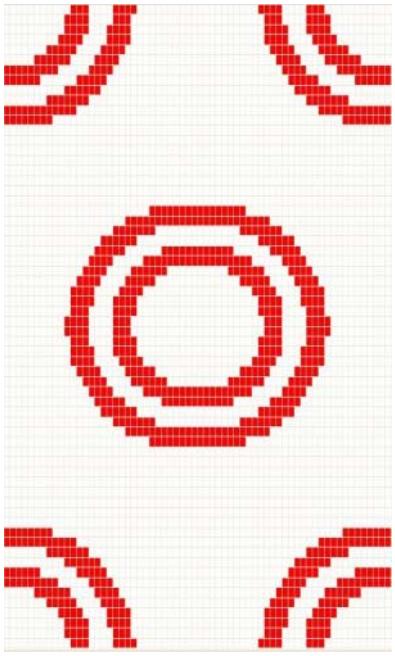

Figure 10. Unit cell (64 x 64) for dual-ring Ka add-on grid.

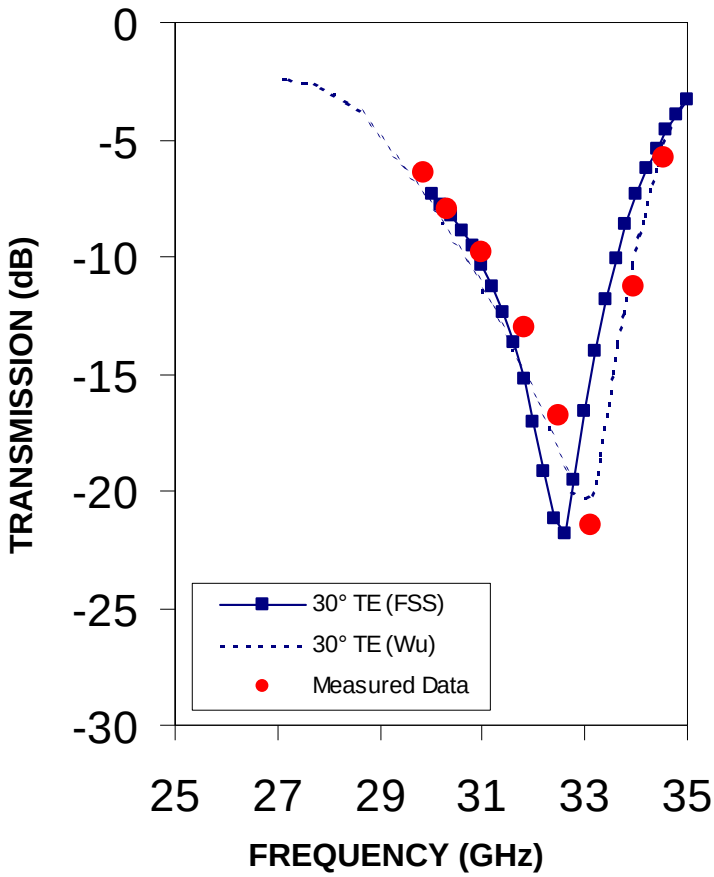

Figure 11. Transmission coefficient as a function of frequency (θ = 30°).

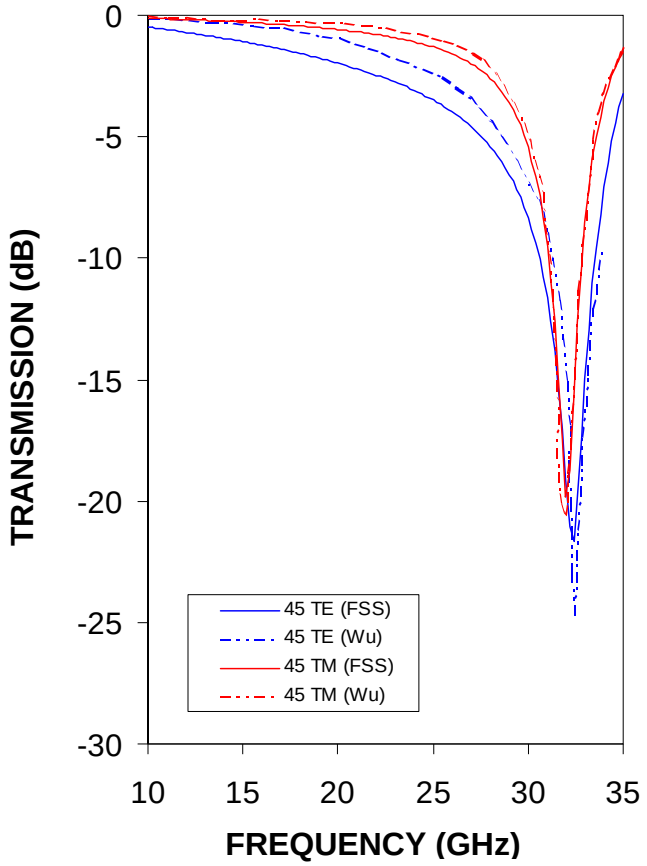

Figure 12. Transmission coefficient as a function of frequency (θ = 45°).

3.1.4 Single-Screen Three-Frequency-Band FSS with Double-Ring Patch Elements

This test case analyzes a single FSS screen in which two circular loops form the basic element, as in the previous example. The elements are arranged on a grid with a skew angle of 60° (Figure 13). The FSS in this example allows RF energy propagation in the S- and Ku-bands while providing a high degree of rejection in the X-band [7]. In Figure 13, the unit cell is highlighted in red on a non-skewed grid. The dimensions, as labeled in the figure, are D = 0.280 inch, r_1 = 0.132 inch, r_2 = 0.0866 inch, W_1 = 0.005 inch, and W_2 = 0.008 inch. Figure 14 shows the FSS unit cell.

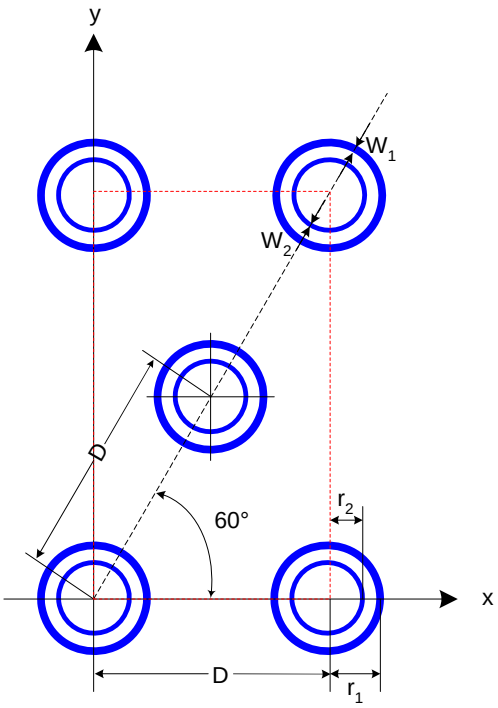

Figure 13. Unit cell consisting of dual rings arranged on triangular grid.

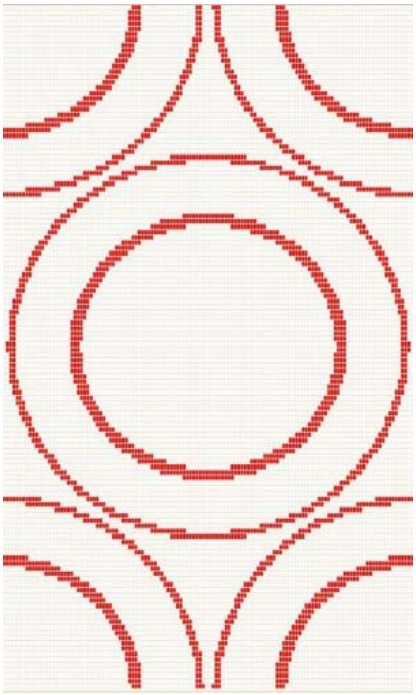

Figure 14. Unit cell used for simulation of dual-ring FSS (128 x 128 discretization).

The transmission coefficients were calculated by using the FSS M&E code for TE and TM polarizations at two incidence angles over a 0.1- to 15-GHz frequency range. The reflection coefficients were also calculated by using FSS M&S; however, in this case, no data were available for comparison. The ratio of transmitted power to incident power provides the transmission coefficient. Figure 15 shows the transmission coefficient as a function of frequency in this band for polarizations at 30 and 45° angles. The results obtained with the FSS M&S are compared with results published in the open literature and were obtained by using the integral equation modal approach with the thin-wire approximation. Solid lines indicate the FSS calculated data and dashed lines indicate the corresponding modal analysis data. All curves predict a deep null at around 8 GHz. For the 30° TE case, FSS M&S predicts the null at 7.85 GHz versus 8.5 GHz, a difference of about 7%. The corresponding values for the 45° TM case are 8.0 and 8.5 GHz, again, a less than 6% difference. The differences are acceptable when comparing the results of two numerical simulations. The difference may be due to the thin-wire approximation, which does not include radial variation for ring expansion.

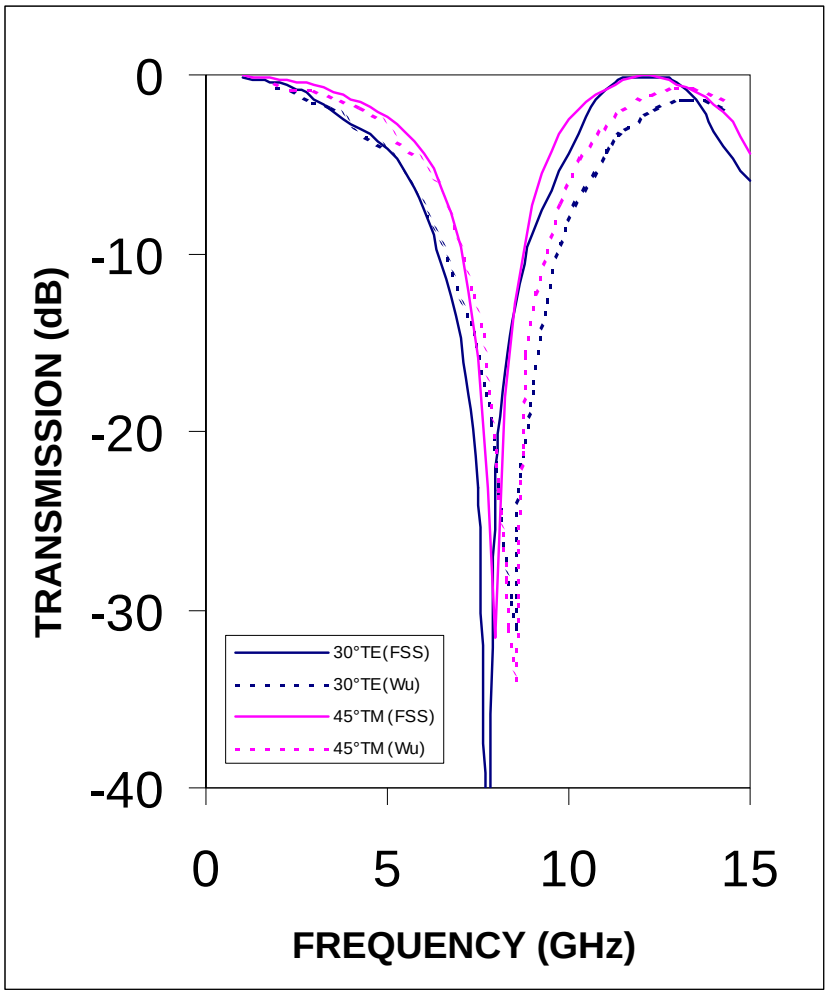

Figure 15. Transmission response for single-screen tri-band FSS.

3.1.5 Dual-Screen Four-Frequency Band (S-/X-/Ku-/Ka-) FSS

This example was part of a case study for the National Aeronautical and Space Administration's (NASA) Cassini mission [9], which was launched in 1997. The spacecraft requires multiple RF frequencies (S-, X-, Ku-, and Ka-bands) for science experiments and data communications links. A single dual-focus, high-gain antenna incorporating an FSS ub_reflector was designed. The subreflector passes S- and Ku-band energy to the prime focus while reflecting X- and Ka-band energy to the Cassegrain feed point. This performance is achieved by cascading two FSS screens in the subreflector. In this test case, the Ka add-on grid, which reflects the Ka-band signals while passing S-, X-, and Ku-band signals, is combined with the single-screen, three-frequency-band FSS examined in Subsection 3.1.4. The three-frequency FSS then reflects X-band signals while passing S- and Ku-band signals. This combination results in a four-frequency-band (S-/X-/Ku-/Ka-) FSS [7] that operates from 2 to 35 GHz. Figure 16 shows the combined structure. Figure 17 shows the FSS unit cells used in the dissimilar FSS M&S engine for the cascaded simulation. Discretization is 64 x 64 for both unit cells.

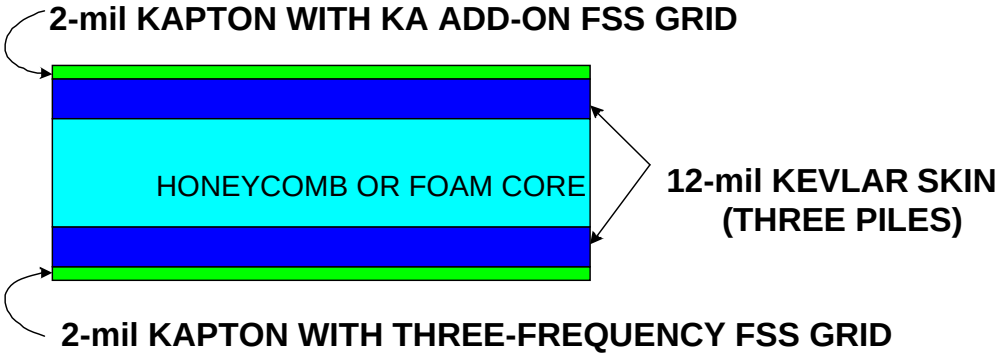

Figure 16. Cross-section of dual-screen S-/X-/Ku-/Ka-band FSS.

The transmission coefficients of the integrated structure were calculated by using the FSS M&S code for TE and TM polarizations at a 30° incidence angle over the 0- to 16-GHz frequency range. Figure 18 plots four data sets that show the results obtained for the TE polarization by using the dissimilar FSS M&S engine. The solid dark blue curve indicates the FSS M&S prediction, the solid red line is based on the single-mode cascading technique, and the measured data are plotted as red points. Finally, data from a second alternative simulation, in light green, are from PMM. All four data sets indicate a transmission null centered at about 8.5 GHz (8.5, 8.4, 8.44, and 8.7 GHz, respectively). Figure 19 shows the TM polarization data and three data sets. The solid dark blue curve indicates the FSS M&S prediction, the solid red line is based on the single mode cascading technique, and measured data are plotted as red points. Again, agreement is good among the three data sets. For TE and TM data sets, the FSS M&S simulations agree very well with alternative simulations and are nearly a perfect match for the measured data. The data clearly show the passband in the S- and Ku-bands, and the rejection in the X- and Ka-bands (not shown in Figure 19), indicating that this configuration met its design goals.

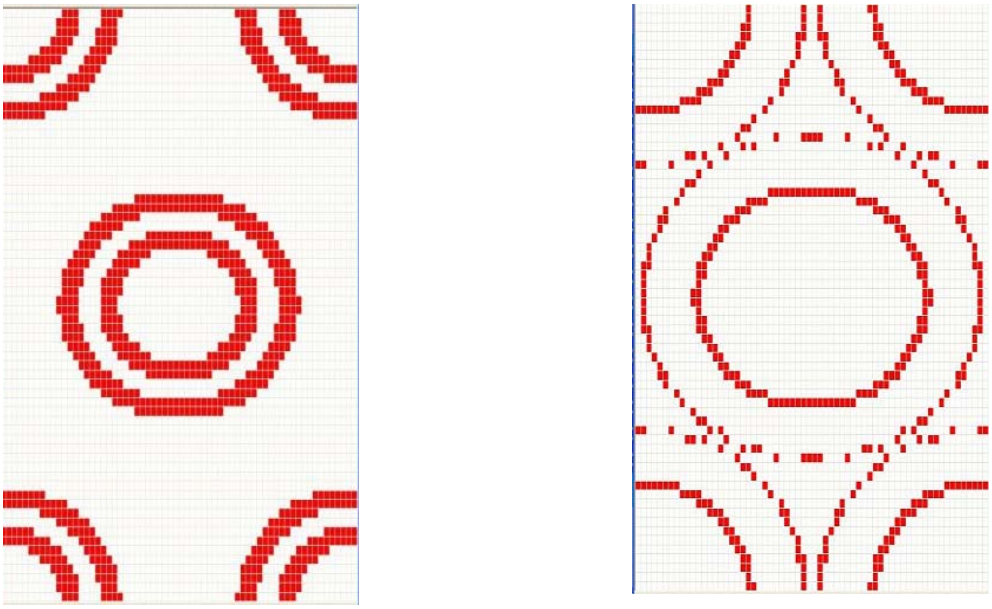

(a) (b)

Figure 17. Unit cells for (a) Ka add-on FSS and (b) three-frequency FSS.

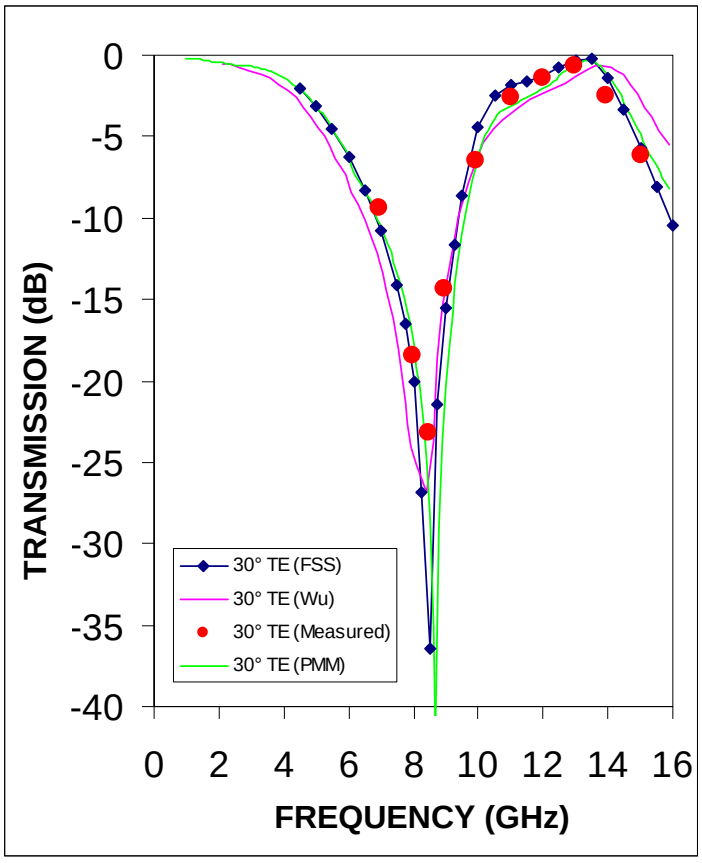

Figure 18. TE transmission performance of cascaded dual-screen FSS.

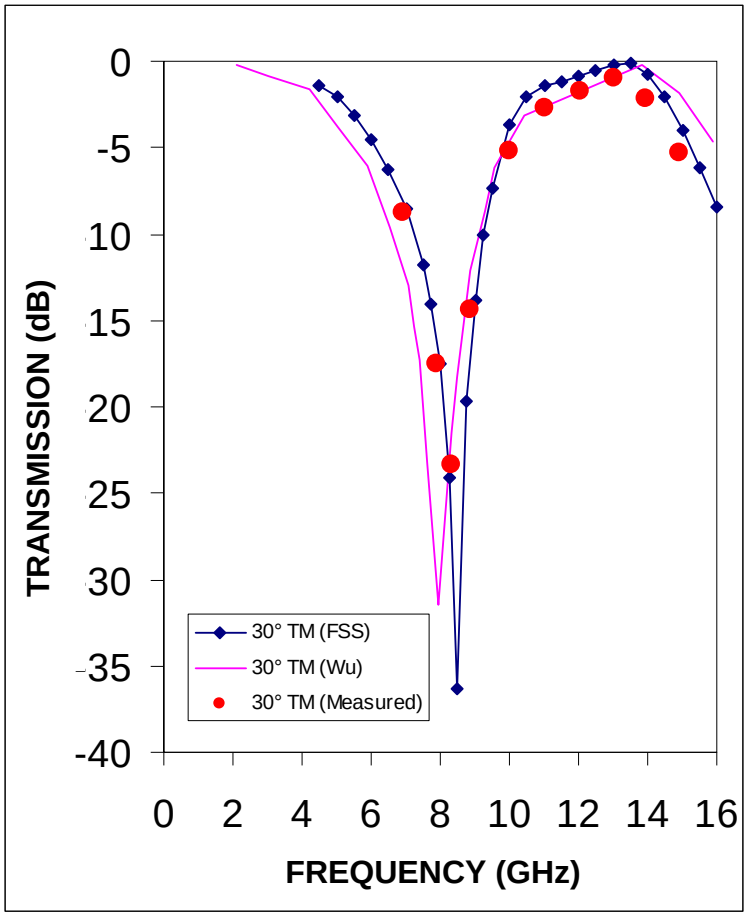

Figure 19. TM transmission performance of cascaded dual-screen FSS.

3.1.6 Gridded Square-Loop FSS

The gridded square-loop FSS is another FSS type that can be used in reflector antennas to provide either dual- or multiple-frequency band operation. This FSS type may be used as curved secondary mirrors in a Cassegrainian configuration or as flat diplexers for feeds co-located at the prime focus. The ideal FSS for this application would be independent of the incidence angle and should introduce minimal cross polarization. The basic element (Figure 20) consists of a square grid of metallization with a square ring contained within each grid. Dimensions, as defined in Figure 20, are W_1 = 0.5588 mm, W_2 = 1.125 mm, P = 8.999 mm, and G = 0.5588 mm [8]. The array has a low-frequency transmission band with a high-frequency rejection band. In this case, we analyze the flat diplexer configuration. (Note that under Fiscal Year 2003 funding, the FSS M&S tool will allow analysis of curved FSS structures.) The FSS elements are printed on 0.076-mm kapton substrates (used in this study) or 0.027-mm polyester substrates. Figure 21 shows two alternative unit cell layouts for the infinite FSS engine. Either unit cell can reproduce the FSS screen; thus, identical results are expected during simulation of the two cases. Identical FSS performance results were achieved; the unit cell in Figure 21(a) was used to obtain the performance data shown later.

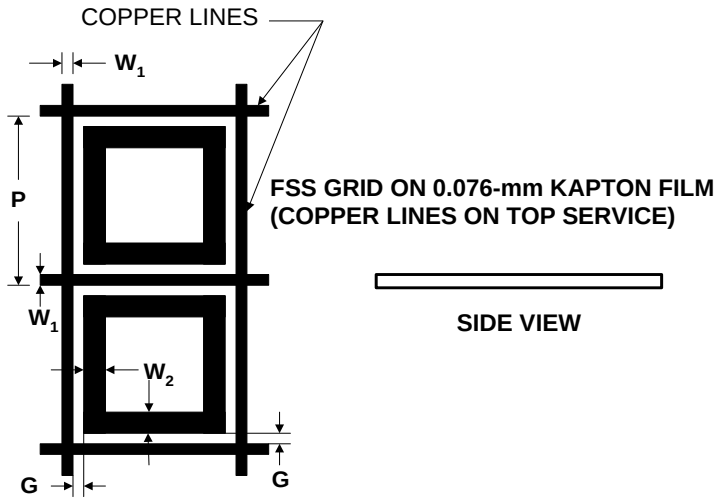

Figure 20. Gridded square loop (layout and cross-section).

The transmission characteristics of these FSS screens were calculated using the FSS M&S code for TE and TM polarizations at 0, 15, 30, and 40° incidence angles over the 6- to 16-GHz frequency range. Figure 22 shows representative data for TE and TM polarizations at an incidence angle of 30°. For each polarization, three data sets exist: FSS (solid line), measured data (points), and numerical data based on an integral equation technique (dashed line). In each data set, a rejection band is observed near 14 GHz. A passband is also evident around an 8-GHz operating frequency. Center frequencies were determined by using the various methods for the rejection band. TE was 14.5, 14.3, and 14.2 GHz; TM was 14.0, 14.0, and 13.9 GHz. In each case, the deviations were within the FSS M&S simulation frequency step-size. The agreement in the curves is quite good with a less than 2% frequency shift for the predicted rejection region. Figure 23 contains TE polarization data for three additional incidence angles: 0° (green lines), 15° (red lines), and 40° (blue lines). The solid lines indicate the FSS M&S predictions while the dashed lines indicate the corresponding integral equation technique predictions. Figure 24 presents similar data for the TM polarization cases. Over the entire frequency range, the FSS M&S and the alternative predictions for all six combinations of incidence angle and polarization were in excellent agreement.

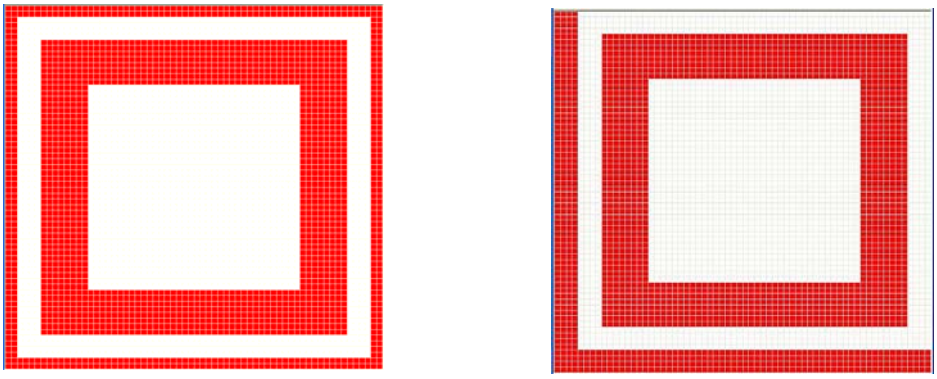

(a) (b)

Figure 21. Alternative unit cells at 64 x 64 discretization.

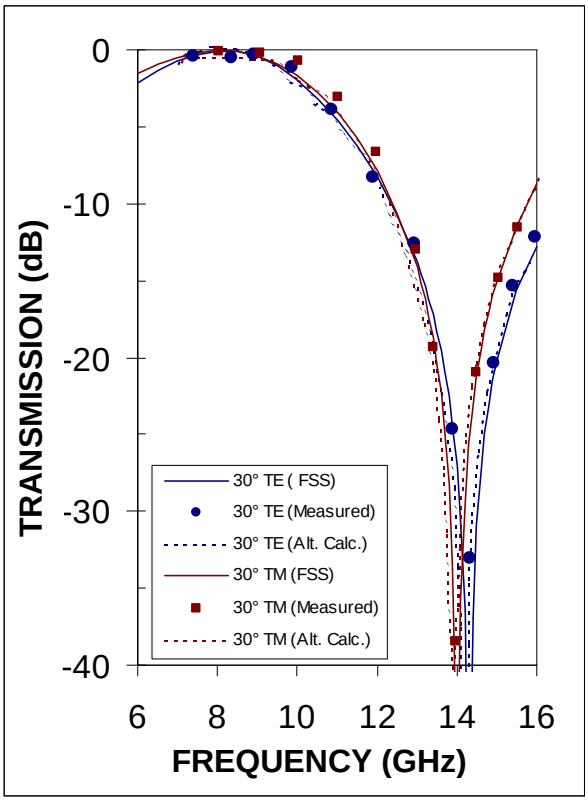

Figure 22. Transmission response for gridded square loop (θ = 30°).

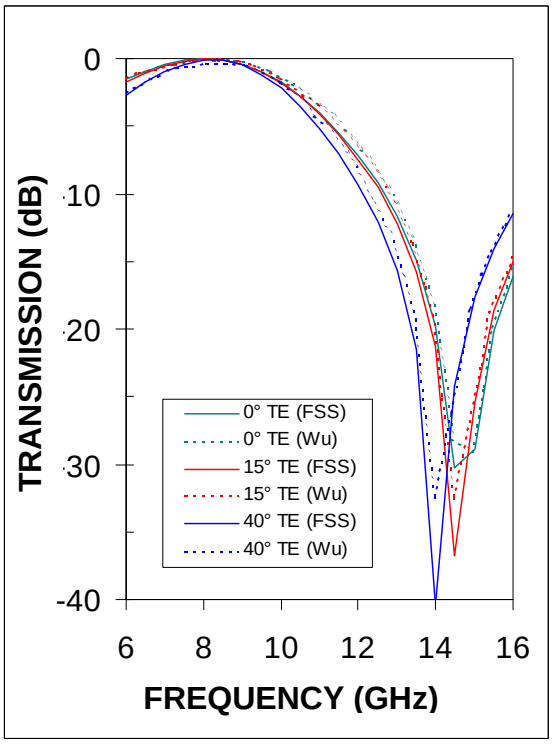

Figure 23. TE transmission response for gridded square loop (θ = 0°, 15°, 40°)

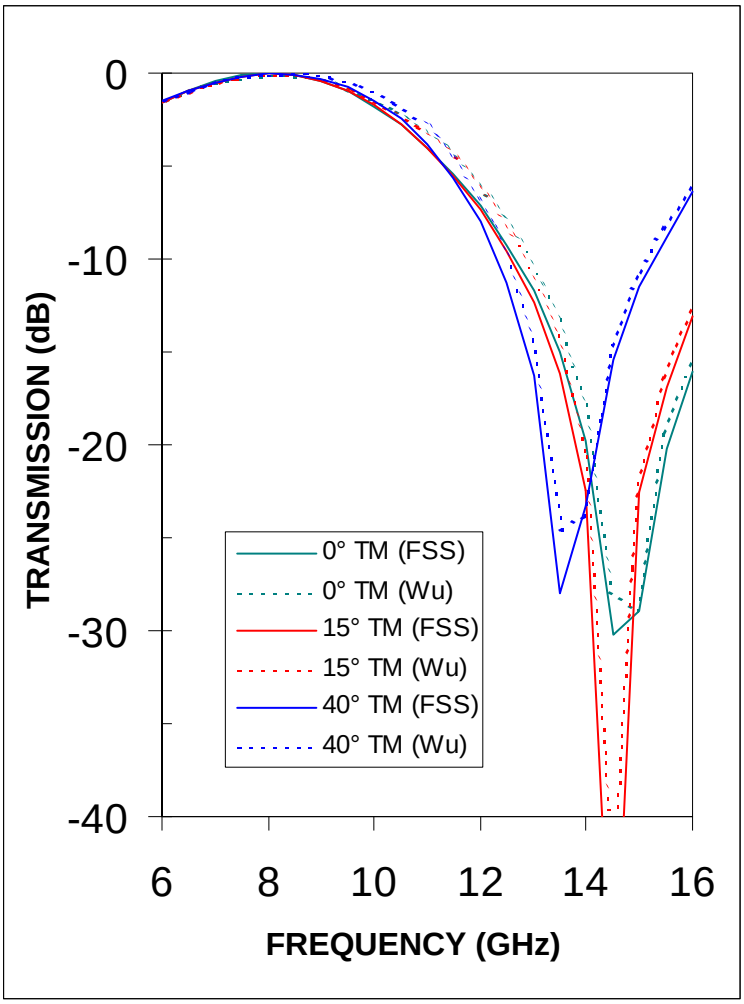

Figure 24. TM transmission response for gridded square loop (θ = 0°, 15°, 40°).

3.1.7 Single-Screen Tri-Band FSS with Double-Square-Loop Elements

The next two test cases were again loop-type elements, but here concentric square ring performance was examined. The first of the two cases analyzed a single FSS screen with each unit cell consisting of two square-loop patch antennas. The unit cell was replicated periodically in two orthogonal directions in the plane of the loops (Figure 25). The FSS elements were printed on one side of the supporting substrate in a planar configuration. The multiple length scales in the unit cell provided resonance conditions at two different frequencies, as with the dual-ring structures. The internal square loop resonates at higher frequencies, while the outer loop dictates the cut-off frequency at the low end. This feature allows a single FSS screen to provide filtering services for two separate communications systems. This particular double-square-loop FSS screen rejects energy in the X-band and propagates energy in the S- and Ku-bands [10].

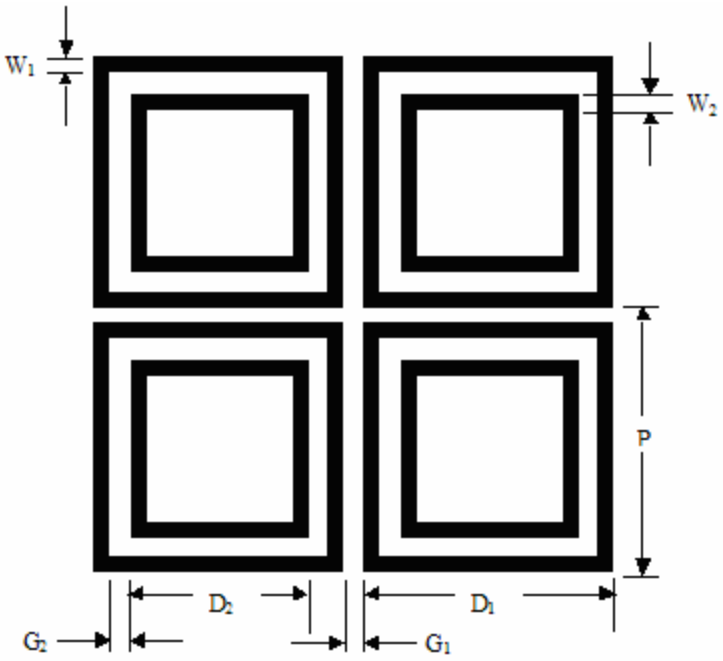

Legend
Period of FSS cell: P = 288 mil
Separation between FSS elements: G_1 = 9 mil
Line width (inner loop): W_2 = 9 mil
Separation gap between inner and outer loops: G_2 = 36 mil
Line width (outer loop): W_1 = 9 mil
Dielectric constant (kapton) = 3.5
Loss tangent = 0.0028
Incident angle: $\theta_i = 30^o$, $\varphi_i = 0^o$, TE polarization

Figure 25. Single screen with double-square-loop element.

The transmission properties of the double-square-loop FSS were analyzed by using the FSS M&S code. Figure 26 shows the FSS unit cell with a 64 x 64 discretization. The reflection data calculated with the FSS M&S is not shown because data for comparison was limited. The FSS performance was characterized for various excitation frequencies, incident angles, and polarizations. Figure 27 shows the transmission responses for several cases as a function of frequency from 2 to 16 GHz. Each case shows a rejection null in transmission at about 8.5 GHz. Solid curves indicate FSS M&S code predictions, dashed curves indicate simulation data based on an integration equation solved by the conjugate gradient method (CGM), and points with a star indicate a second methodology, the equivalent circuit model (ECM). The dark blue data sets indicate 0° TE performance, the magenta data sets indicate 45° TE performance, and the green data sets indicate 45° TM performance. The predicted center frequencies are summarized as follows: 0° TE: 8.25, 8.3, and 8.1 GHz for the FSS M&S, CGM, and ECM techniques, respectively; 45° TE: 8.75 and 8.8 GHz; and 45° TM: 8.75 and 8.6 GHz. The maximum deviation in predicted center frequency was less than 2%. The curves for 0° TE and 45° TM are virtually identical, while the width of the transmission null at 45° TE shows a small discrepancy. FSS M&S predicts a width similar to the other two cases, while the CGM technique predicts a slightly wider rejection bandwidth. Overall, however, data agreement was excellent.

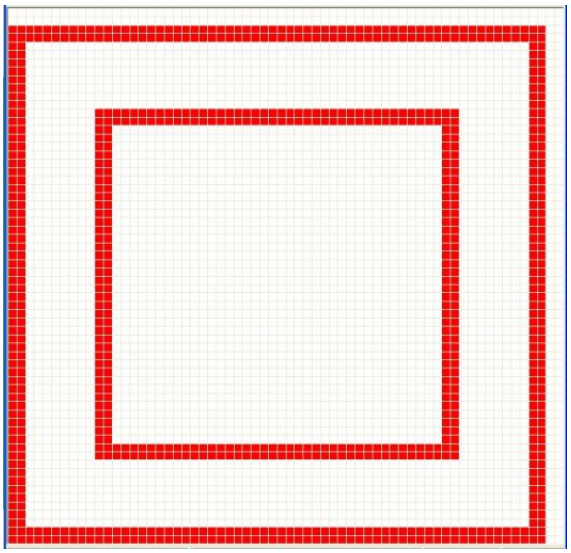

Figure 26. Unit cell for FSS simulation of double-square loop (64 x 64 discretization).

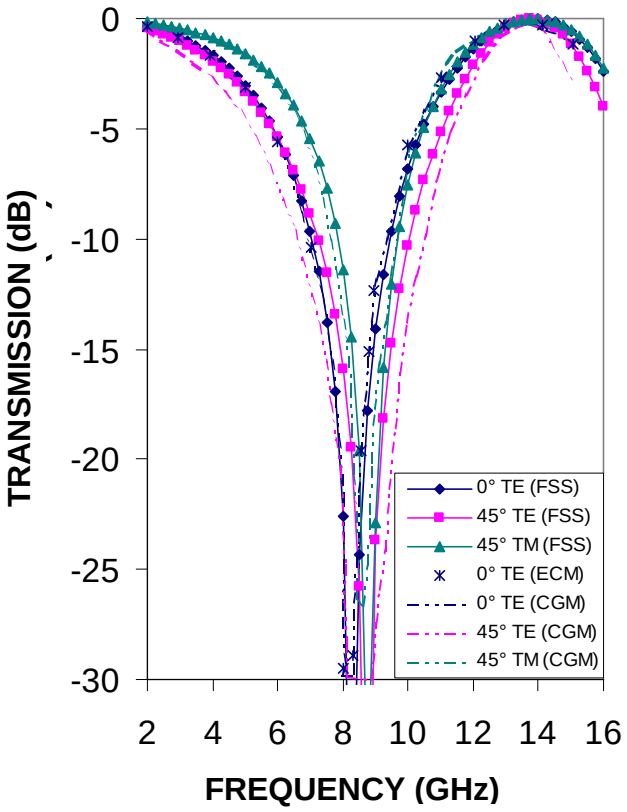

Figure 27. Transmission response of double-square-loop tri-band FSS.

3.1.8 Dual-Screen Four-Band FSS with Double-Square-Loop Elements

This composite was an alternative to the example in Subsection 3.1.5 for achieving the Cassini antenna subsystem's RF goals. The Cassini spacecraft requires multiple RF functions in the S-, X-, Ku-, and Ka-bands. A single high-gain antenna combined with an FSS sub-reflector was designed to meet all these requirements. In this antenna system configuration, two feed points are arranged in a dual-focus reflecting system. The FSS subreflector allows placing both feed points at a focal point of the main reflector. To achieve the desired performance, the subreflector must pass S- and Ku-band energy while reflecting X- and Ka-band energy. This performance is achieved by cascading two double-square-loop radomes in a composite structure with the cross-section shown in Figure 28. The FSS screen at the top, also referred to as "Ka add-on FSS Grids," reflects Ka-band waves but allows S-, X-, and Ku-band energy to propagate through the screen. The FSS screen in the bottom, referred to as the "Three-Frequency FSS Grids," reflects X- and Ka-band waves but passes both S- and Ku-band waves. The operational frequency range is 2 to 35 GHz [10] [11].

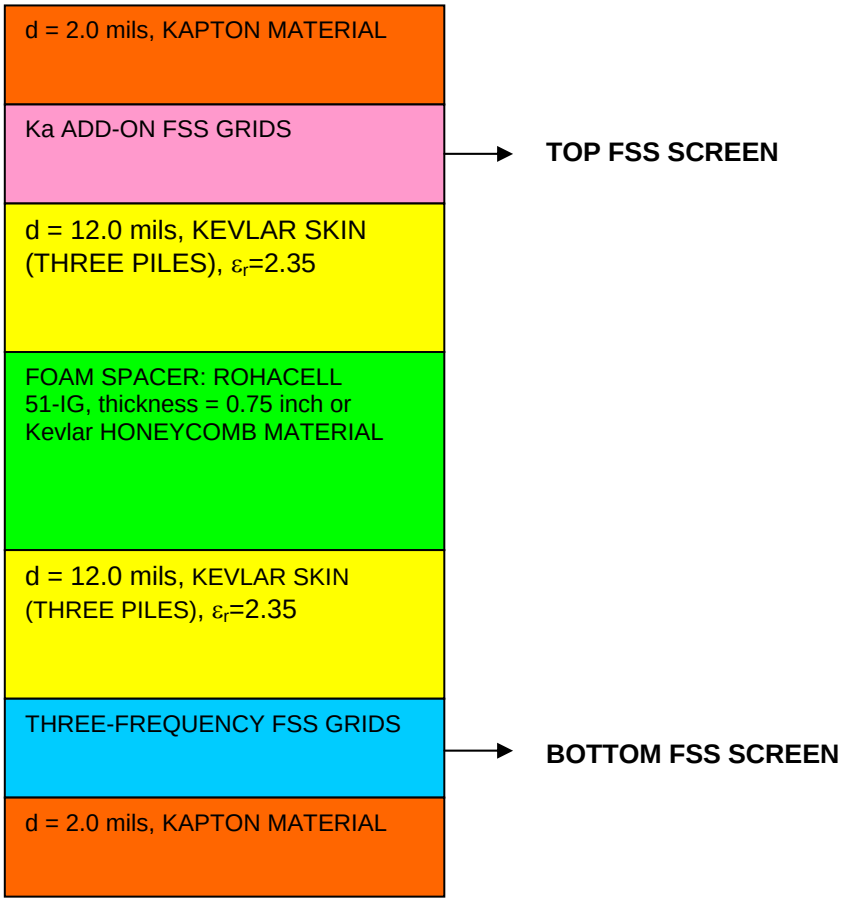

Figure 28. FSS/dielectric layer structure.

Figure 29 shows the geometry of each FSS screen used in this design.

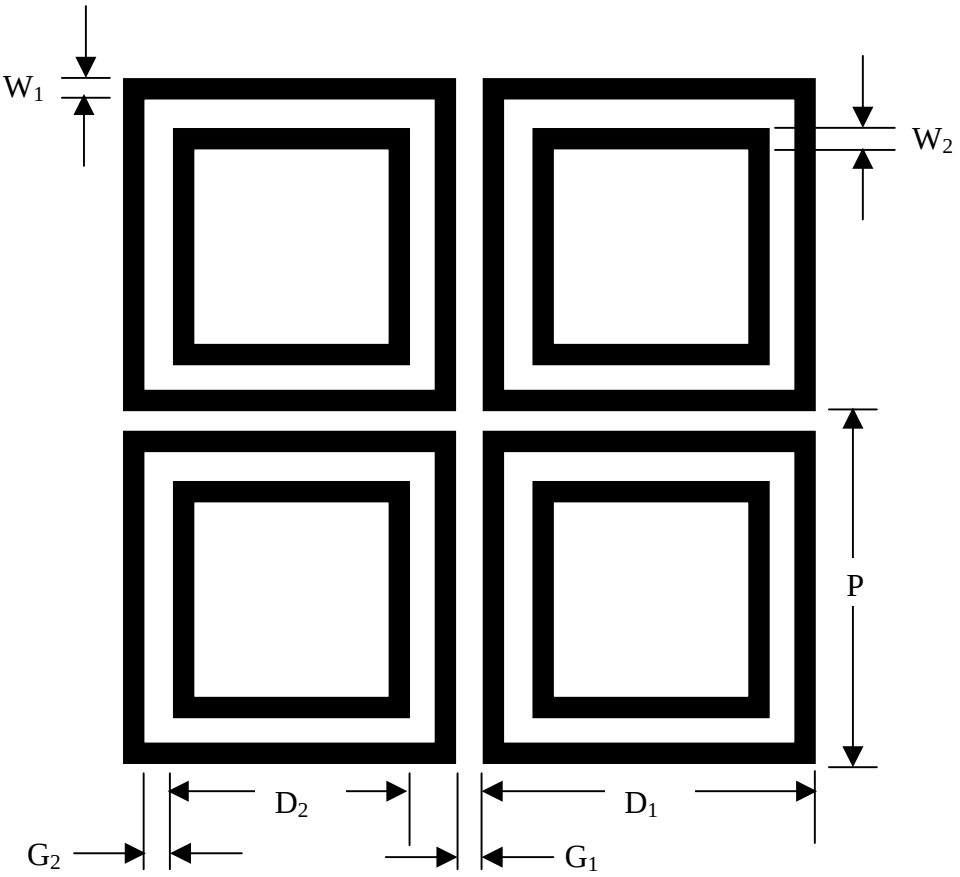

Legend

	Screen 1 (Low Pass) (inches)	Screen 2 (Tri-band) (inches)
	P = 0.112	P = 0.311
	W_1 = 0.007	W_1 = 0.0102
	W_2 = 0.007	W_2 = 0.0307
	G_1 = 0.028	G_1 = 0.041
	G_2 = 0.014	G_2 = 0.0486

Figure 29. FSS unit cell dimensions.

The two FSS screens in the composite are of differing periods. The FSS M&S tool uses an option called dissimilar FSS to perform this type of simulation. The dissimilar FSS M&S code is used to compute the reflection and transmission characteristics of this two-layer, double-square-loop FSS; the characteristics were then compared with data in the open literature. Figure 30 shows the computed and experimentally measured transmission performance of the dual-screen, double-square-loop FSS at normal incidence over the 2- to 35-GHz frequency band. The solid blue curve indicates the FSS prediction of transmission performance from 1 to 16 GHz, the dashed blue line indicates data collected from single mode cascading over the entire frequency band, and the red points indicate experimentally measured data. The data show that multiple passband and rejection band regions can

be achieved with this type of design. For this V&V study, the data for this case were computed up to 16 GHz, a region where alternative numerical and measured data are available. The FSS predicted response was in very good agreement with the other data sets.

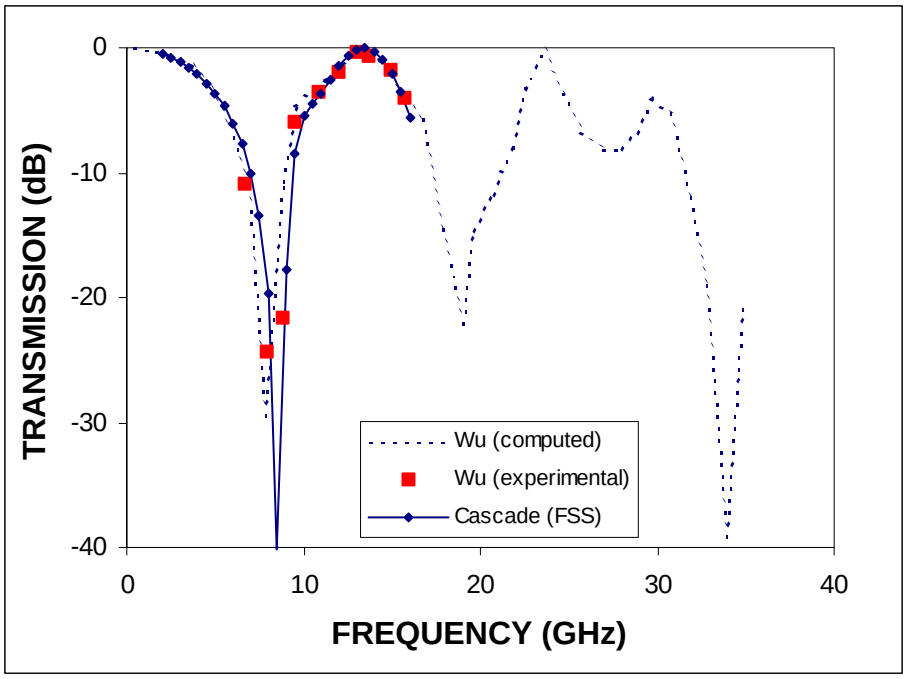

Figure 30. Transmission response for dual-screen double-square loop.

3.1.9 Single-Screen Tri-Slot FSS Spatial Filter

We continue by examining another implementation of center-connected elements. Here, however, the segments are linear slots. This test case considers a tri-slot configuration that, in practice, can achieve circular polarization. As noted previously, FSSs can be used as passive passband structures. The desired frequency response is engineered through dielectic substrates, FSS element configuration, and selection of FSS element type. In some cases, however, the incidence can significantly alter the FSS frequency response. This effect can be used to form a spatial filter that effectively suppresses antenna sidelobes. In this application, it is desirable to maximize the variation in transmission response with incidence angle. In this example [12], the element used was a tri-slot arrayed on a square grid (Figure 31). The dimensions were selected to form a passband at approximately 30 GHz at normal incidence while providing a high degree of rejection at large incidence angles. The FSS elements were formed on a 0.037-mm polyester (dielectric) substrate.

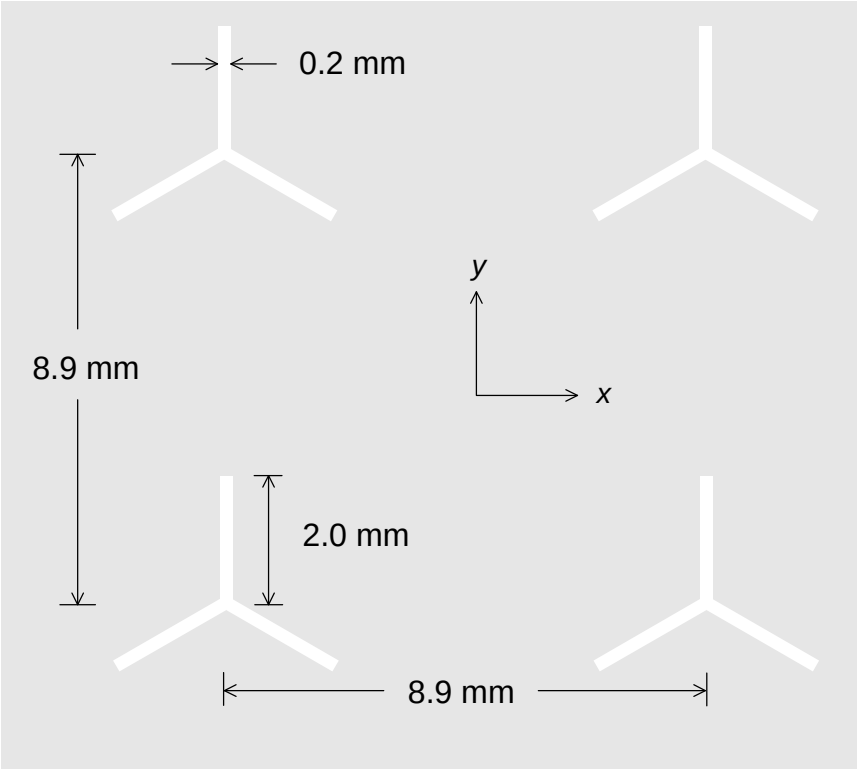

Figure 31. Tri-slot FSS spatial filter layout.

This FSS analysis was initiated with a frequency scan performed at normal incidence from 25 to 35 GHz. Several levels of discretization were considered because of staircasing on the two lower tripole arms (Figure 31). Figure 32 shows the unit cell for each discretization level used, from 64 x 64 to 512 x 512. Figure 33 shows the results of this scan. Each curve shows a clear maximum in transmission response near the middle of the frequency scan. The peak shifts to higher frequency as the level of discretization is increased from 29.7 GHz with 64 x 64 discretization to 30.2, 30.4, and 30.6 GHz for 128 x 128, 256 x 256, and 512 x 512, respectively. Note, however, that this level is a 3% or less variation in predicted transmission maximum across the range of discretization levels, and so 64 x 64 discretization is used for much of the subsequent analysis. Figure 34 shows the measured data on transmission response as a function of incidence angle from 0 to 60° at 30.5 GHz for TE polarization.

To present a valid comparison, the frequency corresponding to the peak value of transmission coefficient for a given discretization level was used for the scan of incident angles. In other words, for a 64 x 64 discretization level, 29.65-GHz radiation was implemented. Similarly, a 30.2-GHz frequency was used in the 128 x 128 simulation. The red curve indicates measured data, the green curve indicates the 64 x 64 FSS M&S prediction, the blue curve corresponds to the 128 x 128 FSS M&S prediction, the brown curve indicates numerical data from a modal analysis, and the magenta curve is the prediction based on the method of moments. The trend is similar for each data set—a slow roll-off from the transmission maximum at normal incidence to about –10 dB at a 55° incidence angle. The simulations predict a 3-dB half-beamwidth of approximately 12°, while the measured data indicate a 3-dB half-beamwidth closer to 18°. Note that an additional calculation based on a modal analysis method also predicts a 3-dB level of about 12.5°. Figure 35 shows TM

polarization data corresponding to the data plotted in Figure 34. The TM polarization data are distinctly different from the TE polarization data. Here, the trend is a sharp drop-off in transmission to about –13 dB at about 5°, followed by a gradual increase in transmission to about –7 dB at 60°. The 3-dB half-beamwidth is predicted to be about 4°, while the measured data indicate a 3-dB half-beamwidth closer to 1°. The various simulations and measured data are in good agreement.

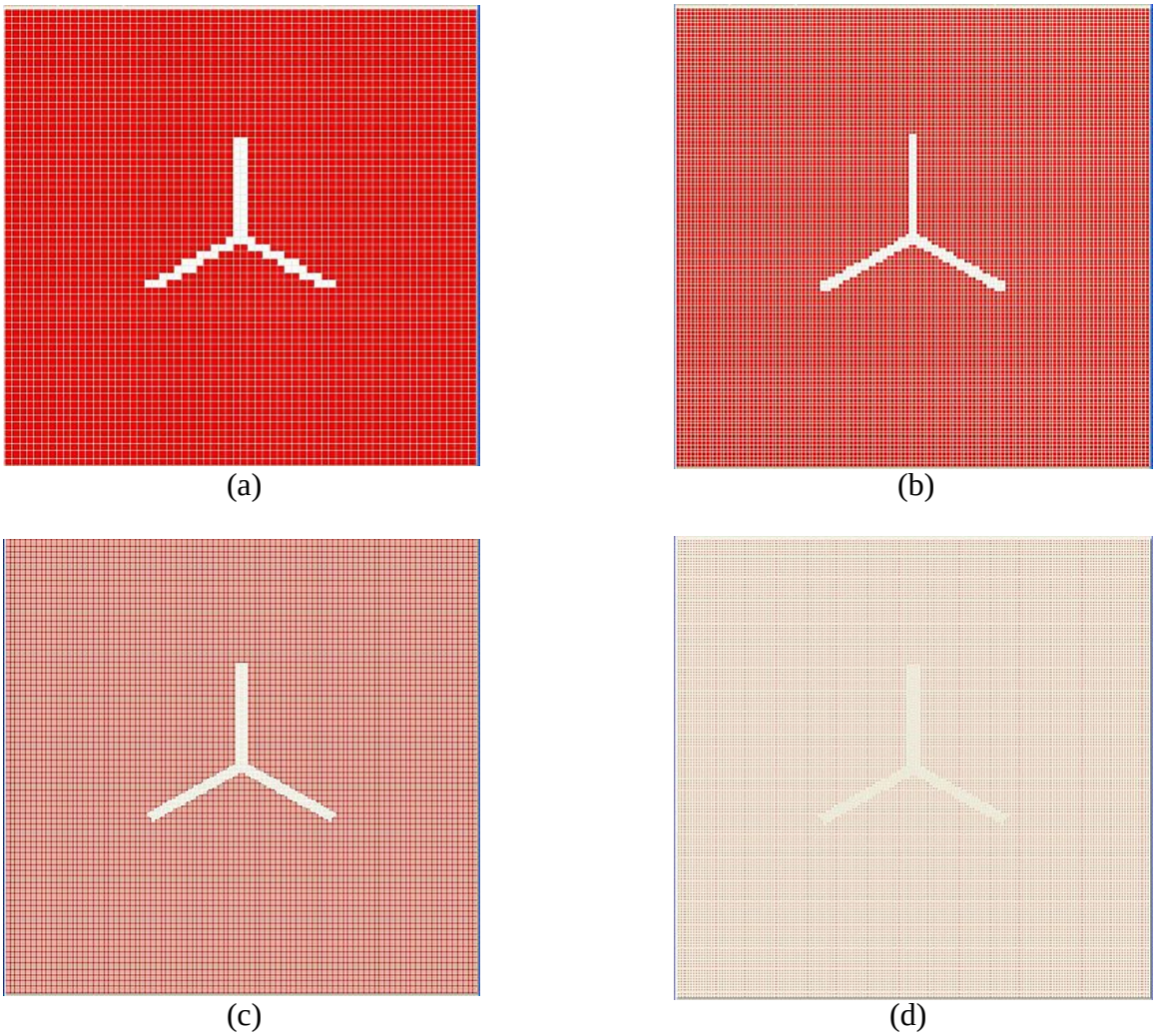

Figure 32. Unit cell at (a) 64 x 64, (b) 128 x 128, (c) 256 x 256, and (d) 512 x 512.

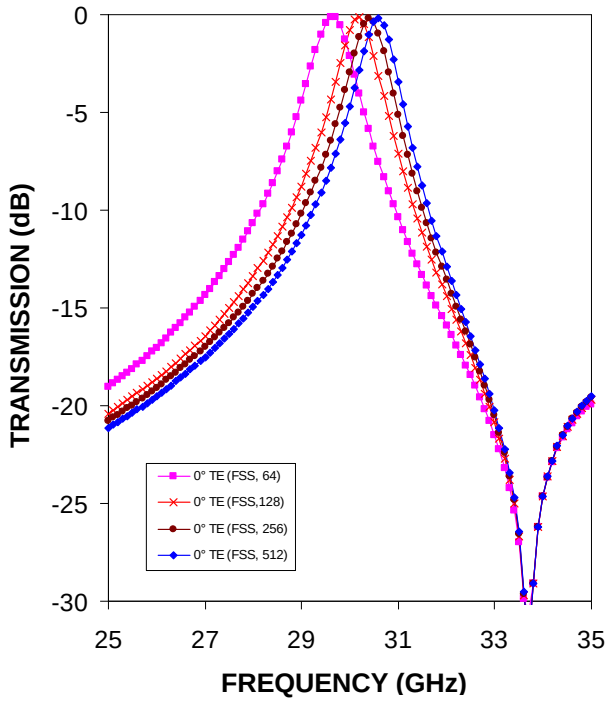

Figure 33. Tri-slot transmission frequency response as a discretization function.

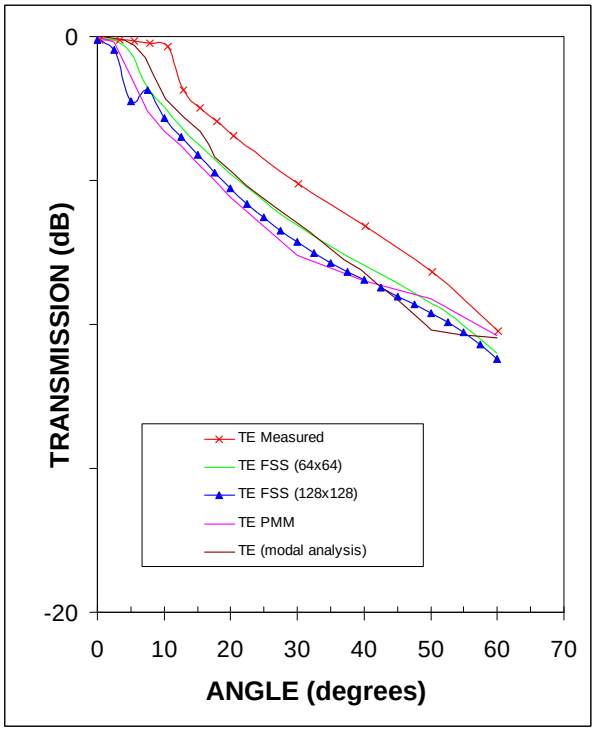

Figure 34. Tri-slot TE transmission response as an incidence angle function.

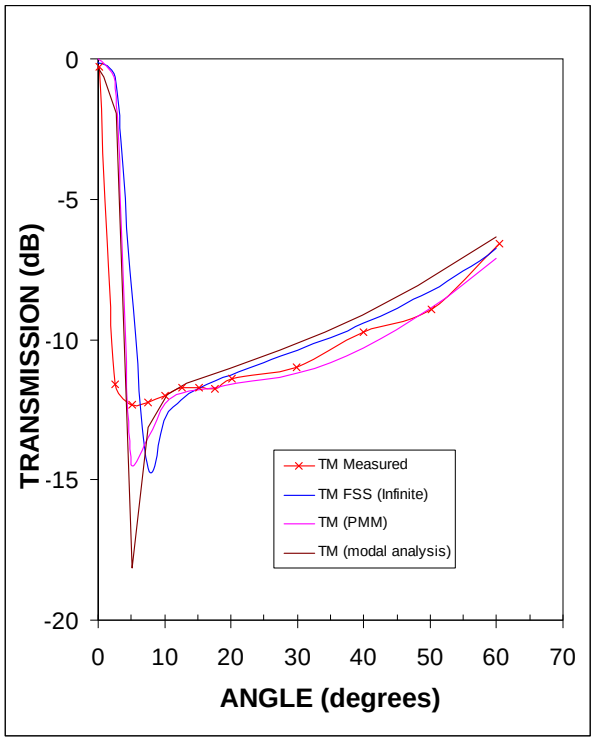

Figure 35. Tri-slot TM transmission response as an incidence angle function.

3.1.10 Single-Screen Cross-Slot FSS Spatial Filter

This example is very similar to the previous example; the difference is that the FSS element is composed of crossed-dipole slots [12] instead of tri-slots. As before, the intent was to demonstrate good spatial filtering characteristics such that a narrow beamwidth with low sidelobe levels could be obtained when used with an antenna. The crossed-dipole elements are arrayed on a square grid with the dimensions and spacings shown in Figure 36. The elements are printed on a 0.037-mm-thick polyester substrate. Figure 37 shows the unit cell for the FSS element with 128 x 128 discretization.

As in the tri-slot example, analysis began with a calculation of transmission performance as a function of frequency over the 25- to 35-GHz frequency band. Results were similar to those in the previous example, with a narrow transmission bandwidth centered at ~30 GHz. One difference is that staircasing effects were not observed in the unit cell layout, as features were aligned with the coordinate axes. Minor differences were observed among different levels of discretization and are attributed to a more accurate representation of the feature sizes. In contrast with the tri-slot case where staircasing is a major effect, the difference between peak positions for 64 x 64 and 128 x 128 discretizations is only 0.15 GHz (0.5%). Therefore, a discretization level of 64 x 64 was used for the rest of the analysis. Since the transmission peak rolls off sharply on either side, the center frequency was used for comparison with the published data. Transmission responses were therefore calculated by using the FSS code as a function of incidence angle from 0 to 60° at 29.4 GHz for the 128 x 128 discretization and 29.55 GHz for the 64 x 64 discretization for TE and TM polarizations.

Figure 38 shows the comparison of transmission response as a function of angle for TM polarization. The figure shows three data sets: the red curve indicated measured data, a solid blue line indicates FSS predictions, and magenta indicates PMM results at 29.8 GHz. All three curves are remarkably similar. As the angle of incidence increases, transmission to about –15 dB at 12.5° decreases sharply. The transmission then increases to about –6 dB at 60°. Figure 39 shows the corresponding TE polarization results. The red curve indicates measured data, a solid blue line indicates FSS predictions, and magenta indicates PMM results. For comparison, brown indicates the 64 x 64 discretization data. The two FSS predictions are nearly identical and very close to the PMM predictions. Both simulations are slightly higher in comparison with the measured data, but all show the same trend—a gradual roll-off in transmission down to about –11.5 dB at 60°.

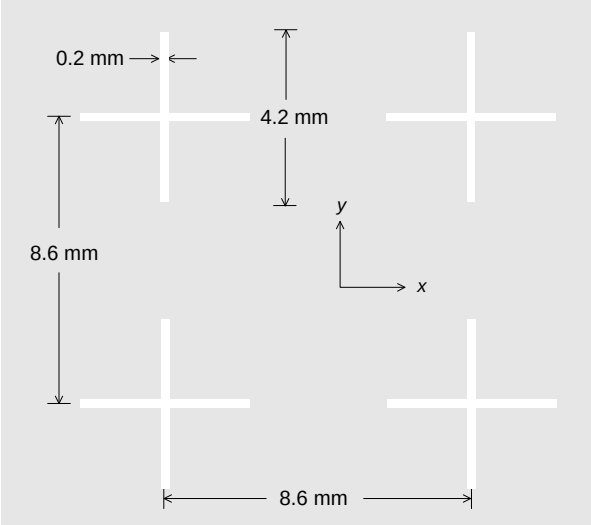

Figure 36. Cross-slot filter layout.

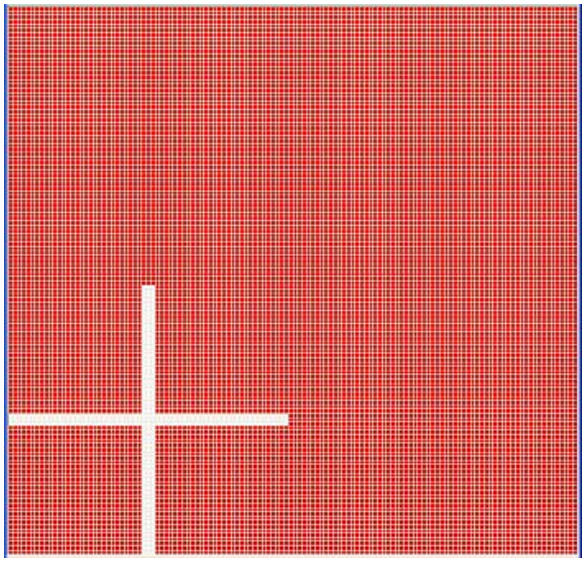

Figure 37. Cross-slot unit cell (128 x 128 discretization).

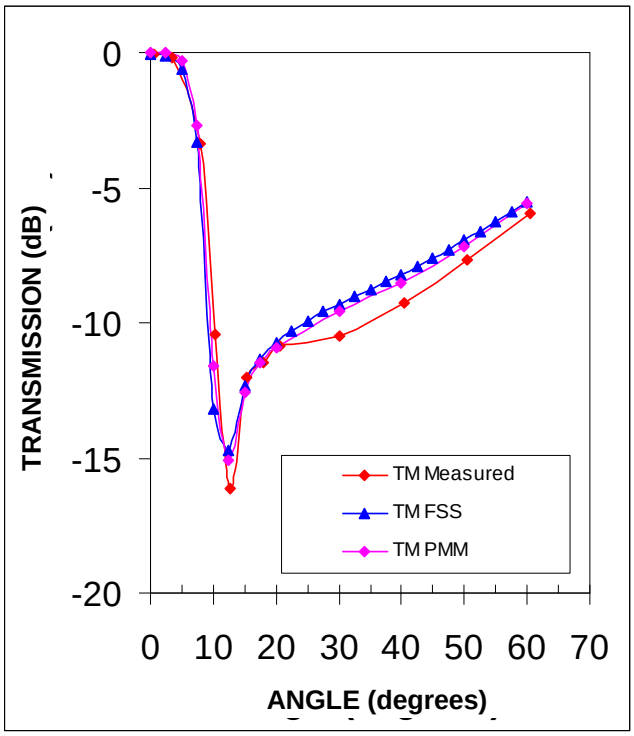

Figure 38. Transmission response as an incidence angle function for TM polarization.

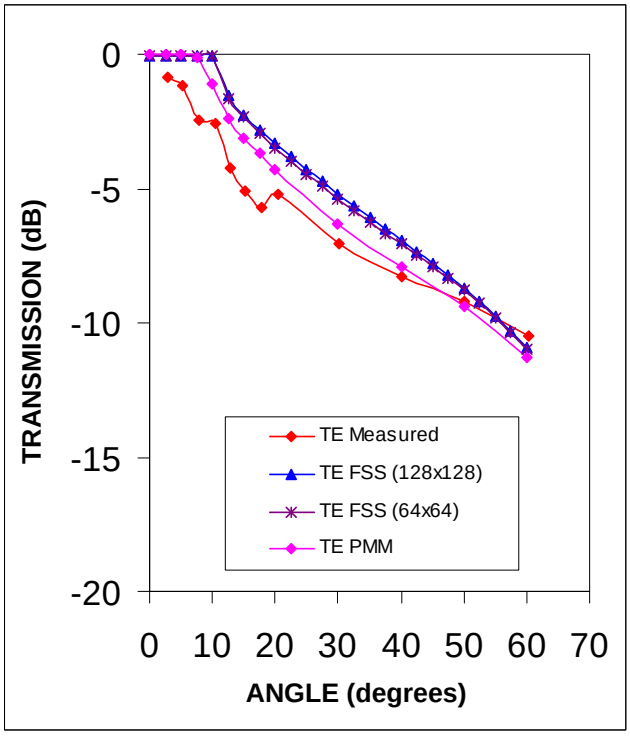

Figure 39. Transmission response as a function of incidence angle for TE polarization.

3.1.11 Bi-Planar Dichroic FSS Filter

This test case examined a filter intended for narrow-band applications. The filter was a composite structure consisting of two identical FSSs embedded within three dielectric slabs. The term dichroic indicates a surface that is transparent in one frequency band and opaque in another frequency band. The element consisted of a four-legged dielectrically loaded cross, another form of loop arranged on a square grid. The filter was designed to be transparent in the 18- to 20-GHz frequency band and reflective from 28 to 30 GHz. Figure 40 (reference [13]) shows the element and FSS structure. The dimensions were W = 0.01389 cm, L = 0.2636 cm, and TW = 0.02718 cm.

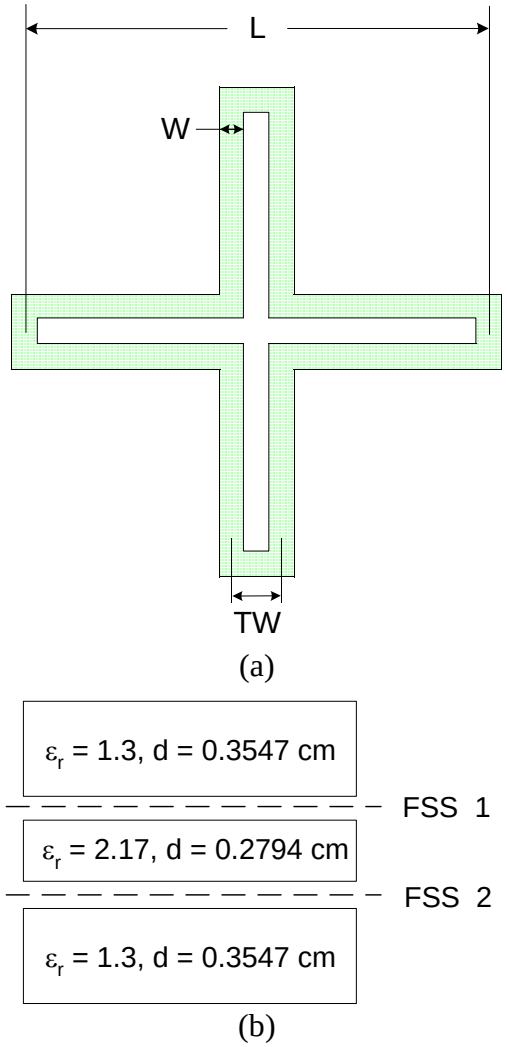

Figure 40. Four-legged, loaded cross: (a) plan view and (b) cross-sectional view.

Transmission and reflection characteristics were calculated by using FSS M&S over the 10- to 40-GHz frequency range at three different incidence angles (0°, 45°, and 60°) for TE and TM polarizations. Two different discretization levels were considered for the unit cell in Figure 41.

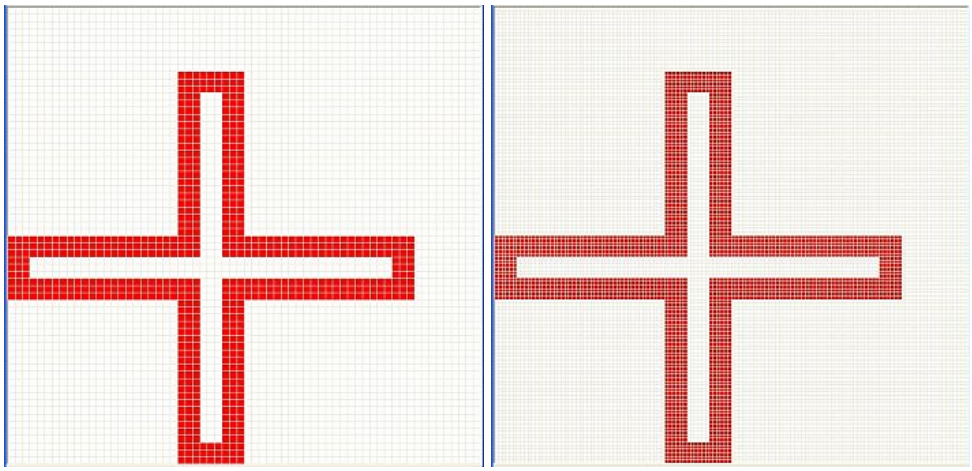

(a) (b)

Figure 41. Discretized unit cells: (a) 64 x 64 and (b) 128 x 128.

The data shown here are for the 64 x 64 discretized unit cell. PMM was used for comparison. Figures 42 and 43 show the transmission response as a frequency function at 0° (blue curves), 45° (red curves), and 60° (green curves) for TE and TM polarizations. Solid lines indicate the FSS M&S simulations and dashed lines indicate the corresponding PMM simulations. In each case, the transmission window shows good agreement at 18 to 20 GHz. At higher frequencies, the reflection window shows that the FSS M&S simulation shifts ~0.7 GHz (~2%) higher than the PMM simulation. The transmission bandwidth is predicted as essentially the same for each corresponding simulation pair. Figures 44 and 45 show the corresponding reflection response data for TE and TM polarizations. The data are represented with the same colors and symbols as above. The curves show a good match, allowing propagation in the 18- to 20-GHz range. The FSS M&S and PMM TE data are closely matched over the 10- to 40-GHz range. The TM polarization data are nearly as good, with some minor differences below the –20-dB level. Overall, this case shows an excellent match between FSS M&S and PMM predictions.

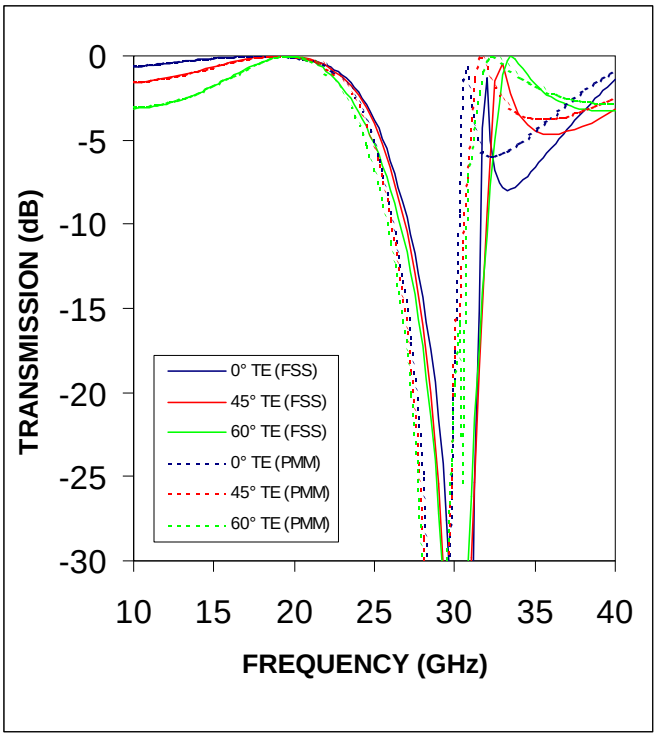

Figure 42. Transmission response for TE-polarized propagation.

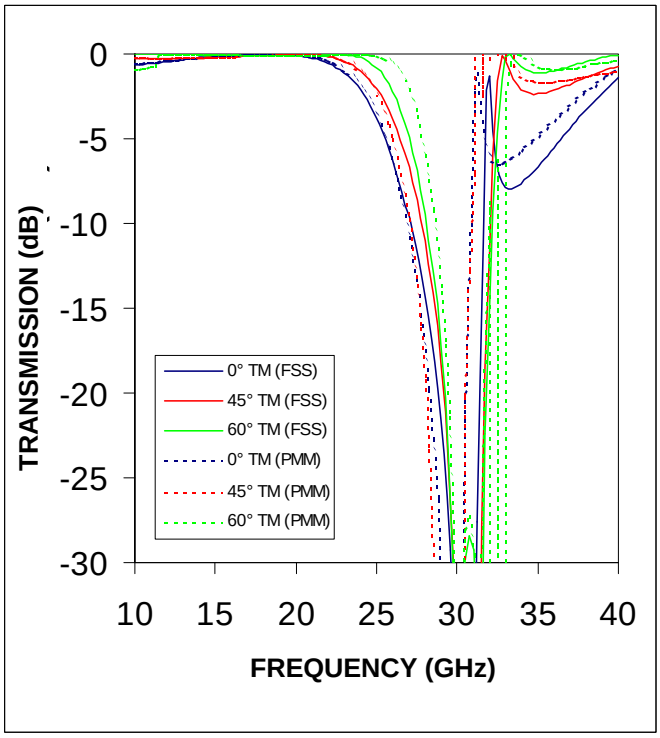

Figure 43. Transmission response for TM-polarized propagation.

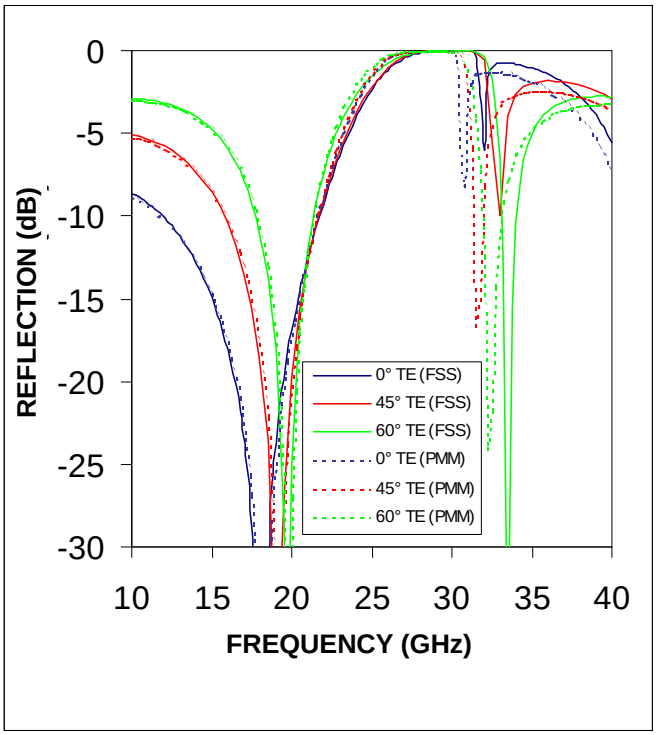

Figure 44. Reflection response for TE-polarized propagation.

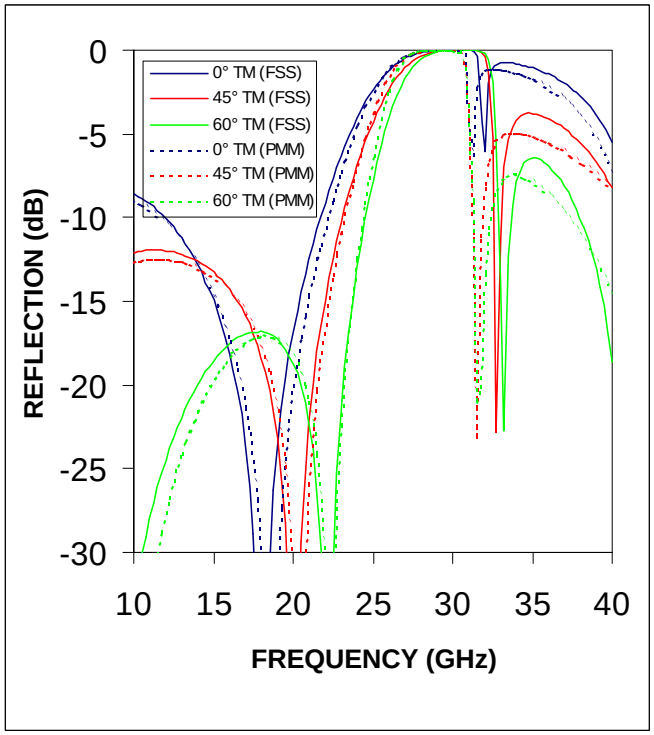

Figure 45. Reflection response for TM-polarized propagation.

3.1.12 Bi-Planar Hexagonal Filter

The hexagonal ring elements in this test case offer unique frequency response characteristics, including the rejection of unwanted signals over a wide bandwidth. In this configuration, the array elements can be closely packed to realize the maximum possible rejection. This particular radome has a band-rejection behavior between 4 and 15 GHz. Figure 46 shows that the FSS elements consist of hexagonal rings arrayed on a triangular grid. The unit cell is outlined in red. The hexagon perimeter = 1.7 cm, the hexagon line width = 0.0171 cm, and the gap between hexagons is 0.025 cm [14]. Two identical FSS screens are sandwiched between five layers of dielectric (Figure 47). The center dielectric layer was simulated at three different thicknesses.

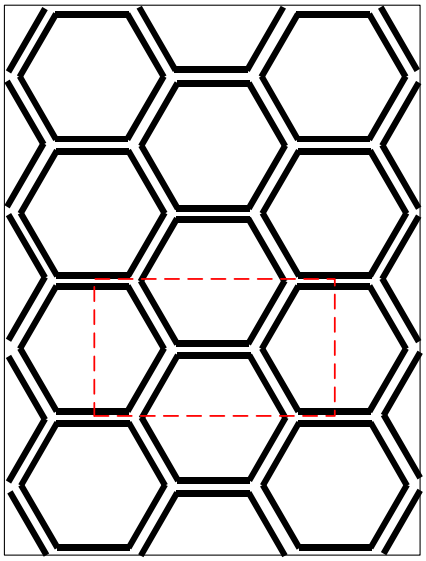

Figure 46. FSS consisting of an array of hexagonal rings.

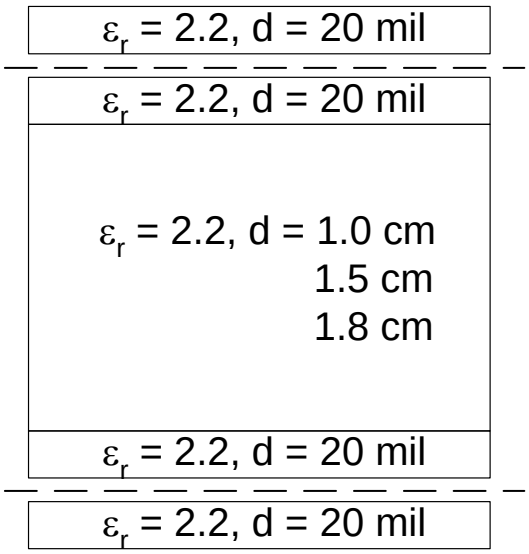

Figure 47. Cross-sectional view of FSS.

Reflection coefficients were calculated for TE and TM polarizations at normal incidence over the 1- to 20-GHz frequency range by using the FSS M&S code and a method of moments technique (PMM). Figure 48 shows the unit cell used for the simulation. Figures 49, 50, and 51 show the simulation results for a center dielectric thickness of 1, 1.5, and 1.8 cm, respectively. In each figure, magenta indicates TE polarizations and blue indicates TM polarization. Solid lines indicate FSS simulations and dashed lines indicate PMM simulations. In each case, the data show the cut-off region at about 4 GHz; a wide rejection band can be designed beyond this frequency. The two simulations are in nearly perfect agreement for each case examined, with a maximum deviation in null location of less than 2%. In all cases, an array interference null is in the middle of the rejection band, mainly because of the coupling between the resonating surfaces, which is expected for this design. Finally, as the center dielectric thickness increases, the array resonances are more closely spaced in frequency; however, the impact on the overall rejection bandwidth is minimal.

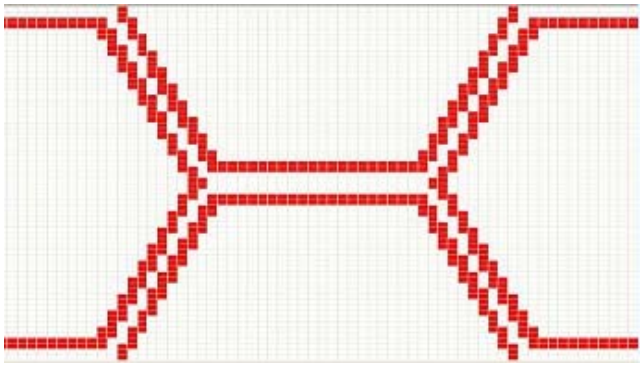

Figure 48. Unit cell (64 x 64); Dx = 0.9126 cm, Dy = 0.522 cm.

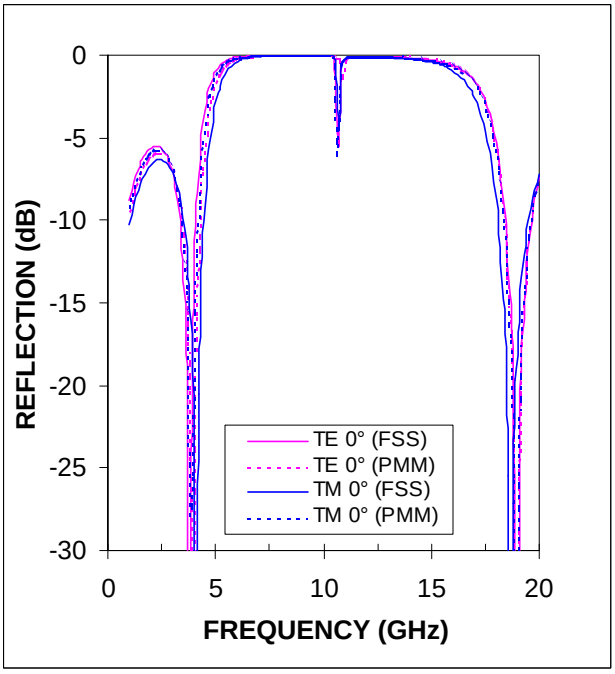

Figure 49. Reflection coefficient curves for FSS (d = 1 cm).

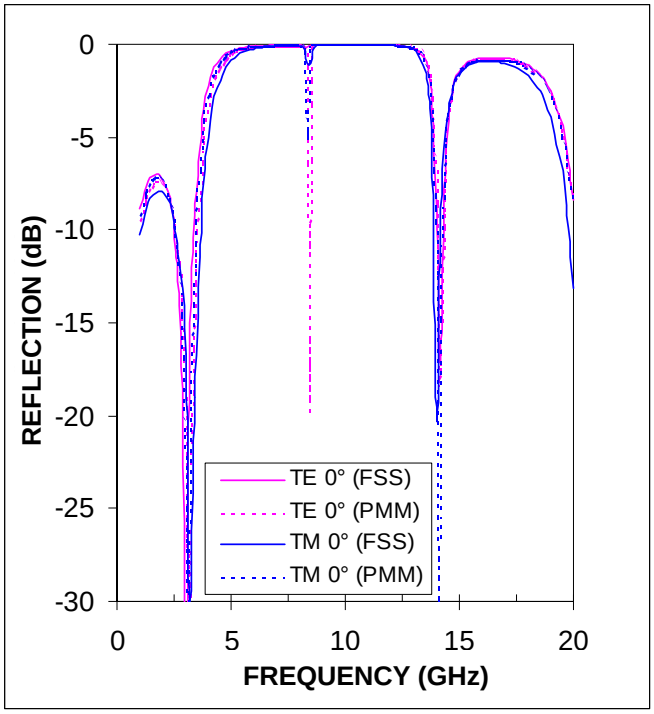

Figure 50. Reflection coefficient curves for FSS (d = 1.5 cm).

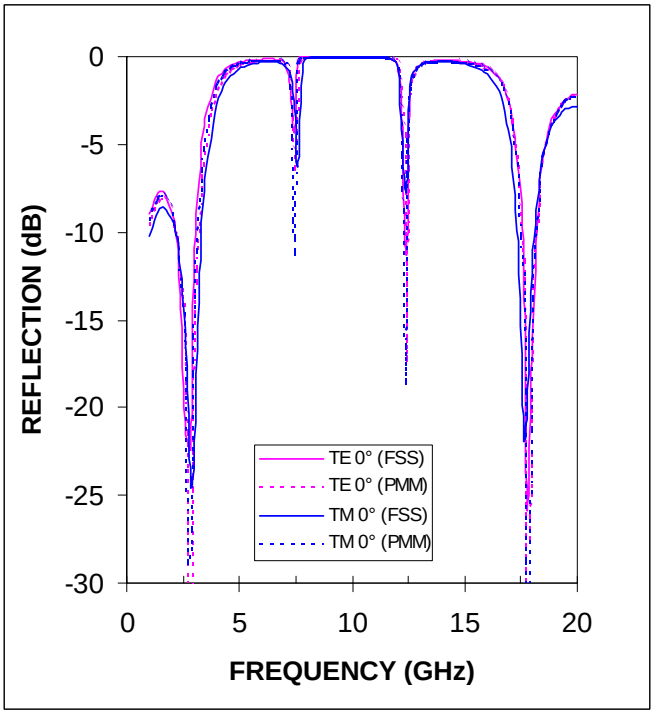

Figure 51. Reflection coefficient curves for FSS (d = 1.8 cm).

3.2 FINITE STRUCTURES

Cases previously examined have focused on infinite FSS arrays. Various element types and multilayer FSS configurations were used to validate FSS M&S capability. As noted previously, all practical FSS structures are finite in extent. In this section, as the next step in the verification and validation process, we examine four of the previous infinite cases in truncated form to evaluate finite FSS radomes. The goal is to examine the impact of the finite boundary condition based on FSS M&S performance analysis. We particularly wanted to determine when it is inappropriate to use the infinite FSS approximation.

3.2.1 Gridded Square-Loop FSS

The gridded square-loop FSS was introduced previously as an FSS that can be used in reflector antenna systems to provide multiband operations. In such applications, the FSS structure can be a secondary subreflector that redirects the RF energy in the desired direction of propagation. In this test case, a flat FSS surface was used to select the propagation path of a given signal. The ideal FSS for these applications would exhibit transmission independent of the incidence angle and should introduce minimal cross polarization. Figure 52 shows the FSS structure layout, which consisted of a square grid of metallization with a square ring contained within each grid. The array had frequency transmission at X-band while rejecting the energy at Ku-band. The structure was a good candidate for circular polarization because of the element layout symmetry. The arrays are printed on 0.076-mm kapton substrates. A 45.7-cm x 45.7-cm experimental FSS array was built and tested [8]. Data from this test article were compared to FSS simulation data.

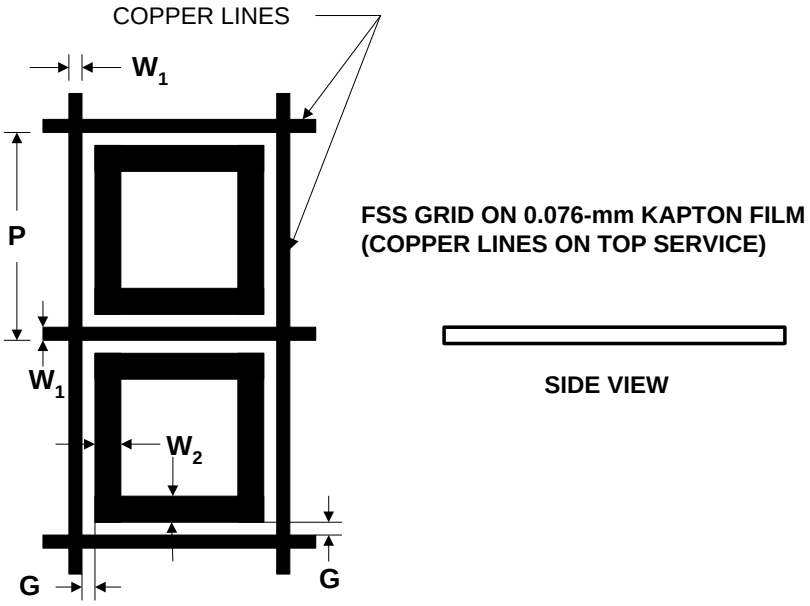

W_1 = 0.5588 mm, W_2 = 1.125 mm, P = 8.999 mm, G = 0.5588 mm

Figure 52. Gridded square-loop FSS layout for finite FSS structure.

The transmission characteristics of these FSS screens were calculated by using the finite FSS M&S code. A 32 x 32 level of discretization was used for the individual elements. Various array sizes were examined. Figures 53 and 54 show the transmission response as a function of frequency for TE and TM polarizations, respectively, at a 30° incidence angle over the 6- to 16-GHz frequency range. The data shown in these figures are from arrays of 7 elements by 7 elements and 22 elements by 22 elements. Each figure shows four data sets; red points indicate measured data, blue (22 x 22) points and light blue (7 x 7) points indicate finite FSS M&S data, and a dashed blue line indicates infinite FSS M&S data. All four data sets show quite good agreement across the entire frequency band for both polarizations. Note that for an array elements of this size (22 elements x 22 elements), the infinite simulation is quite close. Data for the actual array size of 51 elements x 51 elements is indistinguishable from the infinite FSS M&S data. The array of elements can be reduced on the order of 7 x 7 elements before the finite and infinite simulations begin to differ appreciably. The infinite simulation is obviously faster than the finite simulation and the finite simulation calculation time increases as the array size decreases because more spectral points must be sampled as the truncated array size decreases. In this particular test case, the simulation of the 7 x 7 array takes approximately 25% longer than the 20 x 20 array.

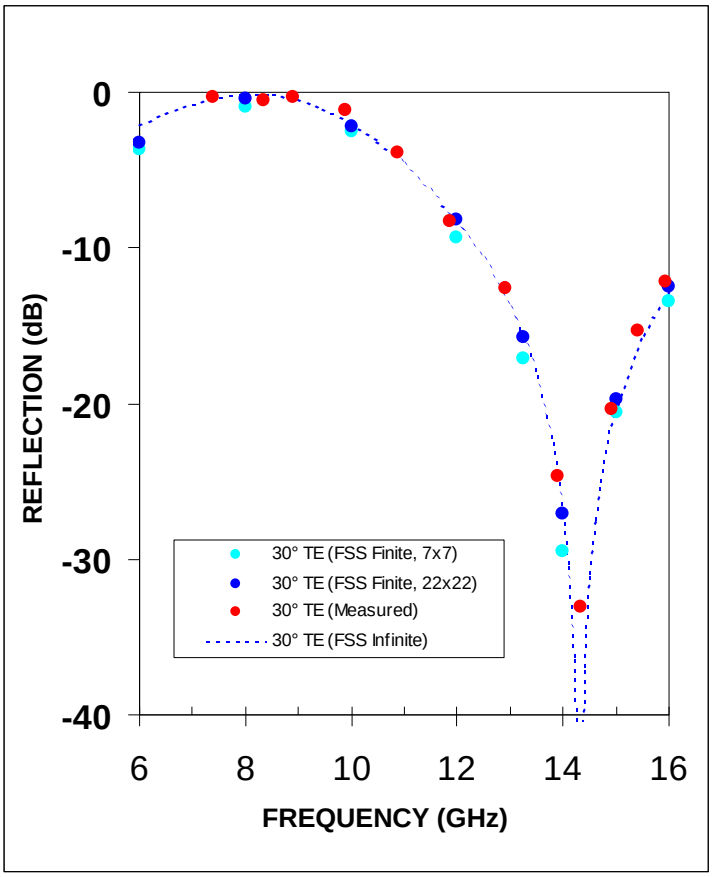

Figure 53. TE transmission response as a function of frequency.

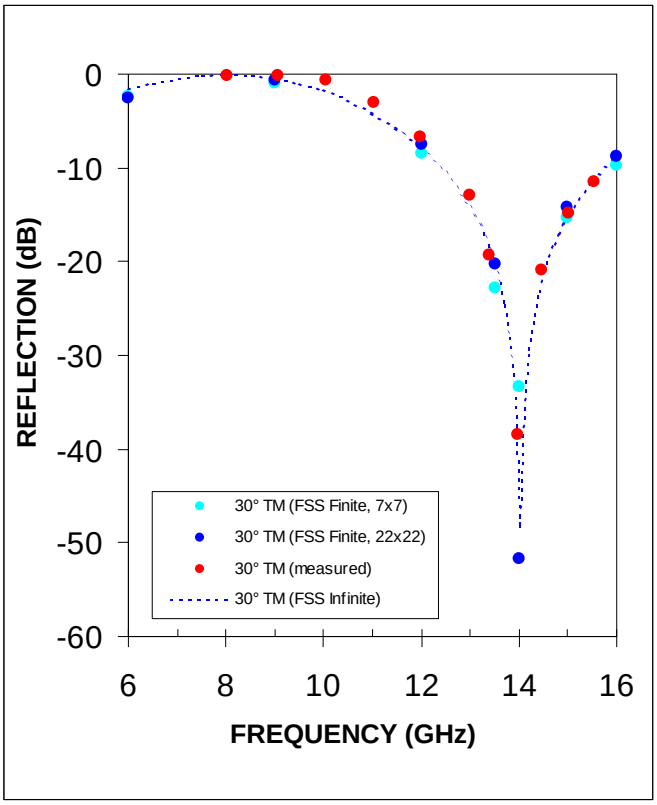

Figure 54. TM transmission response as a function of frequency.

3.2.2 Single-Screen Tri-Band FSS with Double-Square-Loop Elements

This test case analyzed a single FSS screen with each unit cell consisting of two square-loop patch antennas. The unit cell was replicated periodically in two orthogonal directions and in the plane of the loops. These FSS elements were printed on one side of the supporting substrate in a planar configuration. Figure 55 shows the FSS element layout with dimensions. The multiple length scales in the unit cell provide resonance conditions at two different frequencies. The internal square loop resonates at higher frequencies, while the outer loop dominates the low-frequency performance. In practice, this feature can be the basis for a single FSS screen providing filtering services for multiband communication systems. In this test case, a double square-loop FSS screen was designed for transmission in the S- and Ku-bands while simultaneously rejecting energy in the X-band [10].

The propagation characteristics of these FSS screens were calculated by using the finite FSS M&S code for TE polarization at a 30° incidence angle over the 2- to 16-GHz frequency range. The finite data were compared to the infinite FSS predictions. Note that the infinite case was favorably compared with integral equation simulation data in Subsection 3.1.7. Figure 56 shows the TE data. The solid dark blue curve indicates the infinite FSS M&S calculation for reflection coefficient, while the dashed light blue curve indicates the predicted transmission coefficient. The magenta squares and circles indicate the corresponding results for a 128 x 128 finite FSS M&S simulation. The results indicate the presence of a first passband at about 2 GHz (S-band). This particular design has a center rejection frequency in the X-band at 8.25 GHz, with transmission reduced by more than 50 dB. The corresponding reflection coefficient is almost 0 dB, which indicates an almost perfect reflection. As the

operating frequency increases, the radome becomes more transmissive, creating a second passband at 13.8 GHz. This FSS design is clearly designed for transmission at S-band and Ku-band. Data comparison shows that the two numerical simulations yield nearly identical performance. This test case demonstrates that the 128 x 128 size array is large enough for use as an infinite array. From the modeling perspective, infinite case analysis is significantly faster.

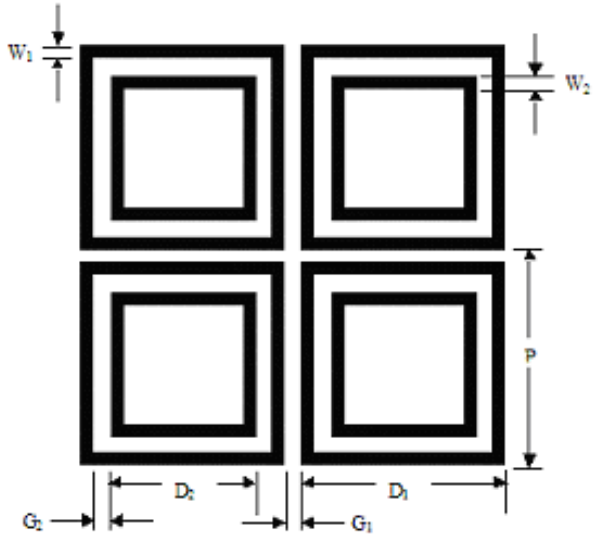

Legend
Period of FSS cell: P = 288 mil
Separation between FSS elements: G_1 = 9 mil
Line width (inner loop): W_2 = 9 mil
Separation gap between inner and outer loops: G_2 = 36 mil
Line width (outer loop): W_1 = 9 mil
Dielectric constant (kapton): = 3.5
Loss tangent: = 0.0028
Incident angle: $\theta_i = 30^o$, $\varphi_i = 0^o$, TE polarization
Array size: 45.7 cm x 45.7 cm

Figure 55. Finite single-screen FSS with double-square-loop element.

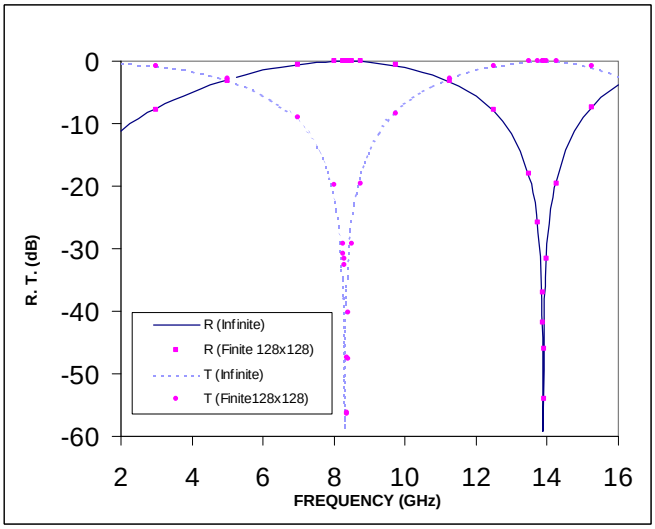

Figure 56. Reflection and transmission responses for finite double-square loop.

3.2.3 Single-Screen Tri-Slot FSS Spatial Filter

As noted previously, the incidence angle can significantly alter FSS frequency response. This effect can be used with an antenna to form a spatially filtered beam with high sidelobe suppression. For this application, it is desirable to maximize the variation in transmission response with incidence angle. In this example [12], the element used was a tri-slot arrayed on a square grid. The element dimensions were selected to form a passband at approximately 30 GHz at normal incidence. Figure 57 shows the FSS dimensions. The actual FSS elements were printed on one side of a 0.037-mm-thick polyester dielectric substrate with a 60- x 60-cm^2 surface.

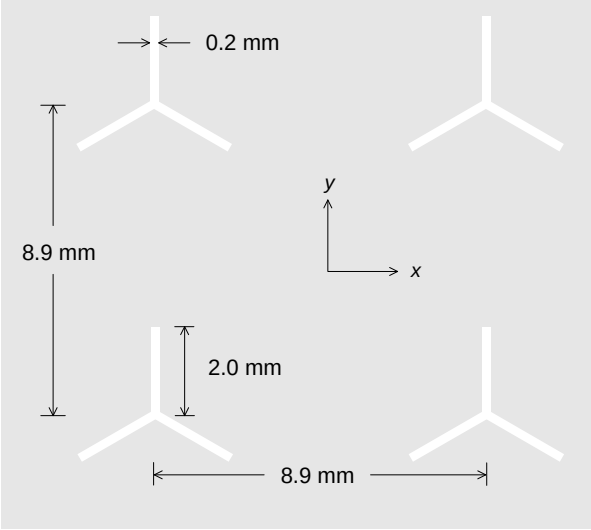

Figure 57. Finite tri-slot FSS layout.

Plane-wave transmission response was calculated using the finite FSS M&S code as a function of incidence angle from 0 to 60° at 29.65 GHz (as previously discussed) for TE and TM polarizations. The FSS is a 68 x 68 array of tri-slot elements. Each unit cell for this test case was modeled with a 64 x 64 resolution. Figure 58 shows the data plots. Blue points indicate the finite simulation results, the green curve indicates the finite simulation results compared with data generated by the infinite FSS M&S code, and the red curve indicates finite simulation results compared with measured data. As the incident angle deviates away from the normal, the transmission coefficient for the TE mode rolls off gradually. At a 60° angle, the transmission coefficient is reduced by 10 dB.

Figure 59 shows the corresponding results for the TM polarization case. Again, three data sets are presented for comparison. The red curve indicates measured data, the blue line indicates the infinite FSS M&S prediction, and the green points indicate the truncated FSS M&S results. Unlike the TE polarization, the TM characteristics show good transmission at normal incidence; however, a sharp drop-off to –13 dB at 5° is observed. Beyond 10°, the transmission rises gradually to –7 dB at 60°. The TE and TM performance is the basis for a spatially filtering FSS. As expected, because of the size of the element array (68 x 68), the finite and infinite FSS M&S simulations are nearly indistinguishable. The results also confirm that substantial rejection of the antenna sidelobes can be realized if an FSS with this type of design is used with the antenna.

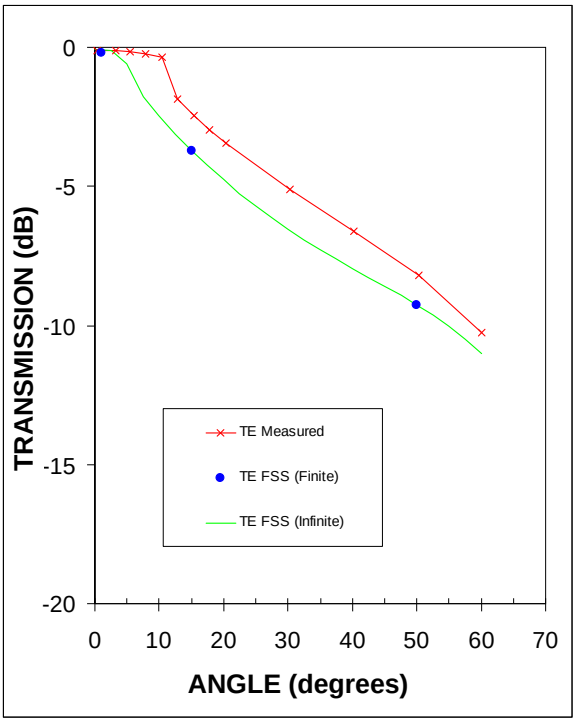

Figure 58. TE transmission response as an angle function.

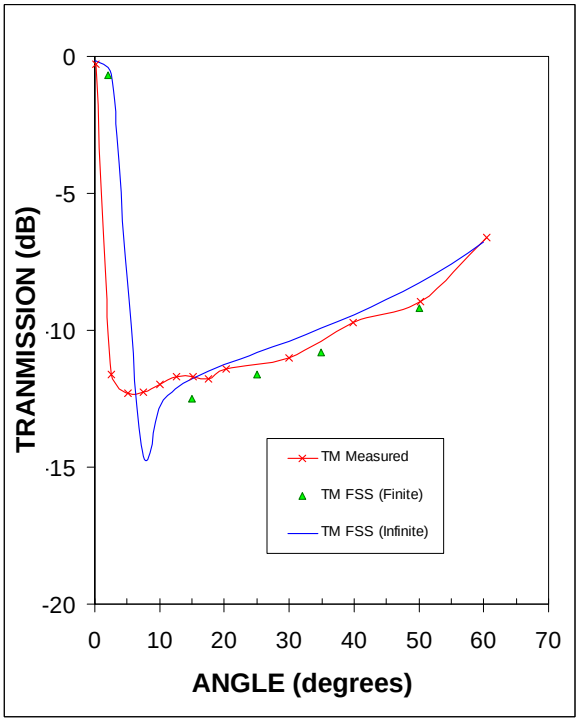

Figure 59. TM transmission response as an angle function.

3.2.4 Single-Screen Cross-Slot FSS Spatial Filter

This final test case is very similar to the previous test case, except the FSS element was composed of crossed-dipole slots in an orthogonal configuration [12]. The purpose was to again demonstrate that good spatial filtering characteristics can be achieved with the appropriate element type, size, and spacing. The crossed-dipole elements were arranged on a square grid. The substrate is a 60- x 60-cm^2, 0.037-mm-thick polyester dielectric film. Figure 60 shows that the total structure contains 4761 FSS elements with unit cell layout and dimensions.

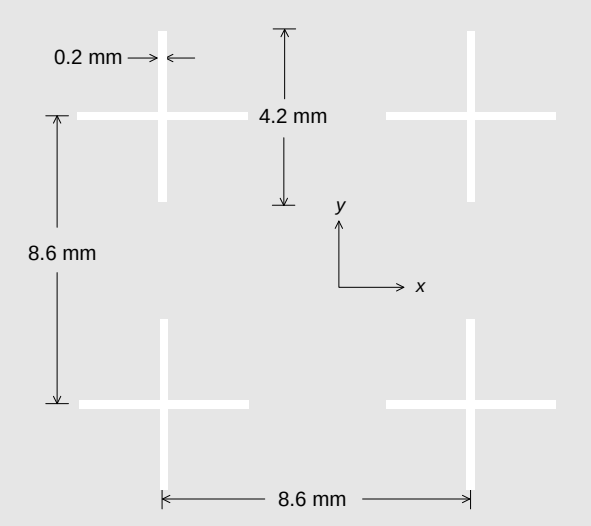

Figure 60. Finite cross-slot FSS layout.

Plane-wave TE and TM transmission responses were calculated using the FSS M&S code as a function of incidence angle from 0 to 60° at 29.4 GHz, as previously discussed in the corresponding infinite case. The finite FSS simulation used a 69 x 69 array of elements, each with a 64 x 64 discretization level. Figures 61 and 62 show the results. A blue line indicates the data generated by the infinite FSS code, while the green triangles indicate finite FSS M&S data. Red indicates the measured data. Each TE data set displays the gradual roll-off in transmission with increasing angle. The maximum transmission is observed at normal incidence. Agreement among the three data sets is good, but they predict a slightly higher transmission value than indicated by the measured data. The TM mode data, on the other hand, show a sharp drop in transmission until 10°, then gradually increase to -5.5 dB at 60° incident angle. These data also show excellent agreement across the entire incident angle range. These specific features can be used to significantly reduce antenna sidelobe levels.

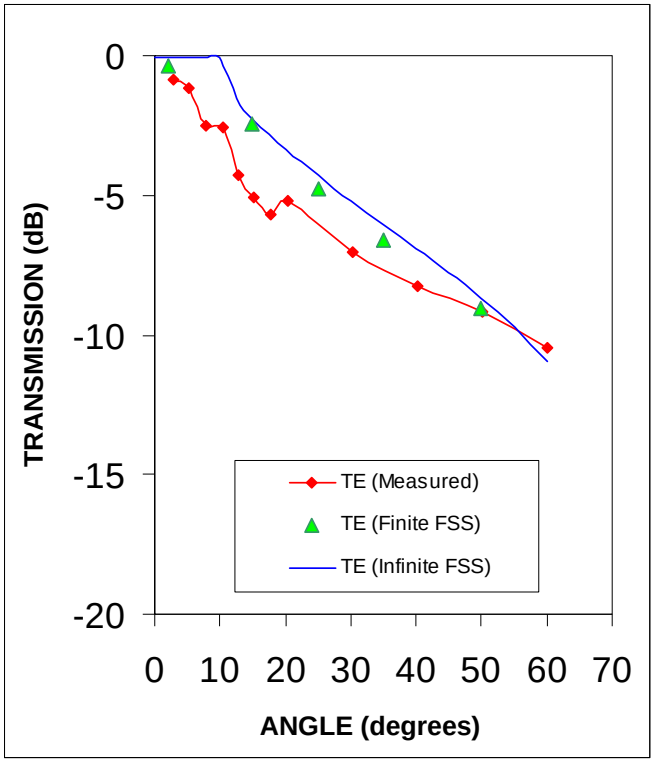

Figure 61. TE transmission response as an angle function.

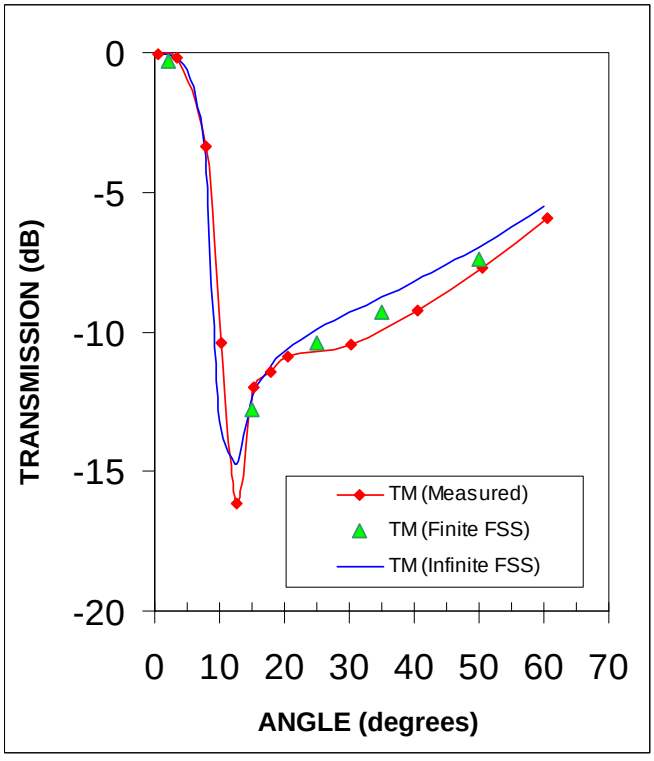

Figure 62. TM transmission response as an angle function.

4. TIMING INFORMATION

When using any M&S tool, it is important that the DD(X) design teams consider the time required to generate a model and run a simulation. To successfully use FSS M&S throughout many design iterations, the computing runtime must be sufficiently fast to quickly simulate design concepts. During this V&V effort, each integrated topside design V&V test case was timed on a Pentium 4 2.2-GHz computer running Microsoft Windows XP Professional®. The computer was equipped with 2-GB RAM and an 80-GB hard drive. Table 2 shows the CPU time (per data point) for these test problems.

Table 2. Computing runtime.

Problem	CPU Time/Point (hh:mm:ss)	RAM (kB)	Discretization
3.1.01	00:00:03.8	2788	64 x 64
3.1.02	00:00:07.9	2788	64 x 64
3.1.03	00:00:14.3	2788	64 x 64
3.1.04	00:12:14.3	7364	128 x 128
3.1.05	00:06:15.6	18652	64 x 64
3.1.06	00:00:16.8	2788	64 x 64
3.1.07	00:00:14.0	2788	64 x 64
3.1.08	00:04:07.1	5752	32 x 32
3.1.09	00:03:11.6	7344	128 x 128
3.1.10	00:05:25.5	7344	128 x 128
3.1.11	00:00:44.7	3404	64 x 64
3.1.12	00:01:02.2	3404	64 x 64
3.2.01	02:41:12.0	5368	32 x 32
3.2.02	02:07:41.0	5368	32 x 32
3.2.03	58:46:56.5	6572	64 x 64
3.2.04	04:15:19.3	5368	32 x 32

Depending on the type and complexity of the problem, the simulation CPU time ranges from a few seconds (test case 3.1.01) to times in excess of 58 hours per data point (test case 3.2.03). Test case 3.1.01 is a very simple infinite FSS structure on a single dielectric layer, while the longest runtime was for test case 3.2.03, which is a finite FSS example that requires a higher discretization level. While these speeds may be adequate for validating code accuracy, improvements in computing performance are, nonetheless, desirable. Note that single processor systems are commercially available with CPU speeds exceeding 3 GHz, along with an increased memory to 4 GB. The increase in processor speed reduces runtime significantly. The increase in memory allows more accurate solutions (i.e., greater number of Floquet modes) on a single computer platform. The future development plan will focus on improvements in runtime efficiency. The Fiscal Year 2004 plan calls for developing a version of the FSS code that is optimized for the Linux® cluster. This capability will significantly reduce the computational time required for radome analysis.

5. CONCLUSION

To address the shortfall in M&S software capabilities for modeling radomes of various types, PEO-DD(X)/PMS-500 commissioned the development of a plan to satisfy these needs. FSS M&S was identified as one of the most promising FSS simulation approaches and was selected for further development. This report presents a summary of the verification and validation of the enhanced FSS M&S code over a wide range of EM test cases, including infinite and finite structures.

Numerous infinite FSS element classes were evaluated during this V&V, including dipole elements, loop-type elements (circular, square, hexagonal, and cross), gridded loops, and slot elements (cross and tripole). FSS structures consisting of elements printed on single, thin dielectric substrates were considered, as were structures with multiple dielectric layers encapsulating the FSS. FSS structures with multiple FSS layers were also analyzed. These structures included cases where the FSS unit cells were identical or incommensurate. The FSS M&S results compare favorably with measured data and alternative numerical techniques.

The FSS M&S tool was used to further analyze selected FSS structures. Gridded structures, loop elements, and slot elements were considered. The radome characteristics predicted by the finite FSS M&S tool showed excellent agreement with the measured data. Based on the cases examined, the infinite solution can be used to adequately approximate finite FSS arrays as small as 7 x 7 in extent.

The FSS M&S V&V was extensive and a significant success. Of the 16 cases investigated, 9 cases have numerical and measured results for comparison. Each test case was selected to verify FSS M&S performance for a specific application or to validate the underlying theoretical framework of the M&S package. No example studied produced less than favorable results. Throughout this study, FSS M&S demonstrated that it could accurately predict the performance of a wide range of radome structures. Based on the reported results, FSS M&S was verified and validated as a capable FSS radome modeling and simulation tool for use within the DD(X) program.

6. REFERENCES

[1] J. G. Maloney and M. P. Keller. 2000. "Analysis of Periodic Structures." In *Computational Electrodynamics: The Finite-Difference Time-Domain Method***,** p. 153. A. Taflove and S. C. Hagness, Eds., 2nd Edition, Artech House, Inc., Boston, MA.

[2] I. S. Sokolnikoff and R. M. Redheffer. 1958. *Mathematics of Physics and Modern Engineering*, pp. 251–254, McGraw Hill, New York, NY.

[3] C. C. Chen. 1973. *IEEE Transactions on Microwave Theory and Techniques*, vol. 21, no. 1.

[4] B. A. Munk. 2000. *Frequency Selective Surfaces: Theory and Design*, p. 29, John Wiley & Sons, Inc., New York, NY.

[5] L. W. Henderson. 1993. "Introduction to PMM, Version 4.0." Technical Report 725347-1, Ohio State University ElectroScience Laboratory, Columbus, OH.

[6] B. A. Munk. 2000. *Frequency Selective Surfaces: Theory and Design*, p. 31, John Wiley & Sons, Inc., New York, NY.

[7] Te-Kao Wu and Shung-Wu Lee. 1994. "Multiband Frequency Selective Surface with Multiring Patch Elements," *IEEE Transactions on Antennas and Propagation*, vol. 42, pp. 1484–1490.

[8] T. K. Wu and W.P. Shillue. 1994. "Dichroic Design for the Orbiting VLBI Earth Station Antenna," *IEEE Proceedings, Microwaves, Antennas and Propagation*, vol. 141, pp. 181–184.

[9] Jet Propulsion Laboratory. 1994. "CASSINI Project Mission Plan," JPL D-5564, Pasadena, CA.

[10] T. K. Wu. 1992. "Single-Screen Triband FSS with Double-Square-Loop Elements," *Microwave and Optical Technology Letters*, vol. 5, pp. 56–59.

[11] T. K. Wu. 1994. "Four-Band Frequency Selective Surface with Double-Square-Loop Patch Elements," *IEEE Transactions on Antennas and Propagation*, vol. 42, pp. 1659–1663.

[12] S. Chandran and J. C. Vardaxoglou. 1993. "Performance of Two Single-Layer FSS as Spatial Filters, *Microwave and Optical Technology Letters*, vol. 6, pp. 339–342.

[13] B. Munk. 2000. *Frequency Selective Surfaces: Theory and Design***,** pp. 307–309, John Wiley & Sons, Inc., New York, NY.

[14] B. Munk. 2000. *Frequency Selective Surfaces: Theory and Design***,** pp. 284–285, John Wiley & Sons, Inc., New York, NY.

REPORT DOCUMENTATION PAGE

Form Approved
OMB No. 0704-01-0188

PLEASE DO NOT RETURN YOUR FORM TO THE ABOVE ADDRESS.

1. REPORT DATE *(DD-MM-YYYY)*	2. REPORT TYPE	3. DATES COVERED *(From - To)*
06–2005	Final	March 2004 to December 2004

4. TITLE AND SUBTITLE

VERIFICATION AND VALIDATION REPORT: FREQUENCY SELECTIVE SURFACE SIMULATION TOOL

5a. CONTRACT NUMBER

5b. GRANT NUMBER

5c. PROGRAM ELEMENT NUMBER

6. AUTHORS

T. Q. Ho, C. A. Hewett — **SSC San Diego**
D. A. Zolnick, M. Kragalott, D. J. Taylor — **NRL**
M. C. Baugher — **NSWC, Dahlgren Div.**
A. K. Agrawal — **Johns Hopkins Univ. APL**

5d. PROJECT NUMBER

5e. TASK NUMBER

5f. WORK UNIT NUMBER

7. PERFORMING ORGANIZATION NAME(S) AND ADDRESS(ES)

SSC San Diego
San Diego, CA 92152–5001

8. PERFORMING ORGANIZATION REPORT NUMBER

TR 1925

9. SPONSORING/MONITORING AGENCY NAME(S) AND ADDRESS(ES)

Naval Sea Systems Command (PMS 500)
1333 Isaac Hull Avenue S. E.
Washington Navy Yard, D.C. 20376

10. SPONSOR/MONITOR'S ACRONYM(S)

NAVSEA

11. SPONSOR/MONITOR'S REPORT NUMBER(S)

12. DISTRIBUTION/AVAILABILITY STATEMENT

Public release; distribution is unlimited.

13. SUPPLEMENTARY NOTES

14. ABSTRACT

To address the shortfall in M&S software capabilities for modeling radomes of various types, PEO-DD(X)/PMS-500 commissioned the development of a plan to satisfy these needs. FSS M&S was identified as one of the most promising FSS simulation approaches, and was selected for further development. This report presents a summary of the verification and validation of the enhanced FSS M&S code over a wide range of electromagnetic test cases, including infinite and finite structures. The verification and validation of FSS M&S conducted under this study was extensive, and can be considered a significant success. Of the 16 cases investigated, 9 cases have numerical and measured results for comparison. Each test case considered in this V&V effort was selected to verify the performance of FSS M&S for a specific application or to validate the underlying theoretical framework of the M&S package. No example studied produced less than favorable results. Throughout this study, FSS M&S demonstrated that it can accurately predict the performance of a wide range of radome structures. Based on the reported results, FSS M&S has been verified and validated as a capable FSS radome modeling and simulation tool for use within the DD(X) program.

15. SUBJECT TERMS

Mission Area: Communications

frequency selective surface, antenna design, modeling, simulation, infinite structures, finite structures, verification, validation, software development

16. SECURITY CLASSIFICATION OF:			17. LIMITATION OF ABSTRACT	18. NUMBER OF PAGES	19a. NAME OF RESPONSIBLE PERSON
a. REPORT	b. ABSTRACT	c. THIS PAGE			Thinh Q. Ho
U	U	U	UU	74	19B. TELEPHONE NUMBER *(Include area code)* (619) 553–3783

INITIAL DISTRIBUTION

20012	Patent Counsel	(1)
21511	S. Baxley	(1)
21512	Library	(2)
21513	Archive/Stock	(3)
2825	T. Ho	(15)

Defense Technical Information Center
Fort Belvoir, VA 22060–6218 (1)

SSC San Diego Liaison Office
C/O PEO-SCS
Arlington, VA 22202–4804 (1)

Center for Naval Analyses
Alexandria, VA 22311–1850 (1)

Government-Industry Data Exchange
Program Operations Center
Corona, CA 91718–8000 (1)